Large-scale RNAi screening uncovers therapeutic targets in the parasite Schistosoma mansoni

Wang, Jipeng; Paz, Carlos; Padalino, Gilda; Coghlan, Avril; Lu, Zhigang; Gradinaru, Irina; Collins, Julie N.R.; Berriman, Matthew; Hoffmann, Karl F.; Collins, James J.

Published in:
Science (New York, N.Y.)

DOI:
10.1126/science.abb7699

Publication date:
2020

Citation for published version (APA):
Wang, J., Paz, C., Padalino, G., Coghlan, A., Lu, Z., Gradinaru, I., Collins, J. N. R., Berriman, M., Hoffmann, K. F., & Collins, J. J. (2020). Large-scale RNAi screening uncovers therapeutic targets in the parasite Schistosoma mansoni. *Science (New York, N.Y.)*, *369*(6511), 1649-1653. [eabb7699]. https://doi.org/10.1126/science.abb7699

Large-scale RNAi screening uncovers therapeutic targets in the parasite *Schistosoma mansoni*

Authors: Jipeng Wang[1†], Carlos Paz[1†], Gilda Padalino[2], Avril Coghlan[3], Zhigang Lu[3], Irina Gradinaru[1], Julie N.R. Collins[1], Matthew Berriman[3], Karl F. Hoffmann[2], James J. Collins III[1]*.

Affiliations:

[1]Department of Pharmacology, UT Southwestern Medical Center, Dallas, Texas 75390

[2]Institute of Biological, Environmental and Rural Sciences (IBERS), Aberystwyth University, Aberystwyth, Wales, UK.

[3]Wellcome Sanger Institute, Wellcome Genome Campus, Hinxton, Cambridge CB10 1SA, UK

[†]Equal Contribution

*Correspondence to: JamesJ.Collins@UTSouthwestern.edu

Abstract: Schistosome parasites kill 250,000 people every year. Treatment of schistosomiasis relies on the drug praziquantel. Unfortunately, a scarcity of molecular tools has hindered the discovery of new drug targets. Here, we describe a large-scale RNA interference screen in adult *Schistosoma mansoni* examining the function of 2,216 genes. We discovered 250 genes with phenotypes affecting neuromuscular function, tissue integrity, stem cell maintenance, and parasite survival. Leveraging these data, we prioritize compounds with activity against the parasites and uncover a pair of protein kinases (TAO and STK25) that cooperate to maintain muscle-specific mRNA transcription. Loss of either of these kinases results in paralysis and worm death in a mammalian host. These studies may help expedite therapeutic development and invigorate studies of these neglected parasites.

One Sentence Summary: An RNAi screen examines the function of 20% of *S. mansoni* genes uncovering new phenotypes and suggesting new therapeutic targets.

Main Text: Studies of gene function in intra-mammalian schistosome parasites have been limited to relatively small numbers of genes(*1*). Therefore, we developed a large-scale RNAi screening platform on adult schistosomes that prioritized a list of 2,320 of the worm's ~10,000 protein coding genes (**Fig. S1A**, **Table S1**). We generated dsRNAs, and treated adult male and female pairs with dsRNA over the course of a 30-day experiment (**Fig. 1A**). After filtering genes that either did not amplify by PCR, or failed to generate sufficient concentrations of dsRNA, a total of 2,216 genes were screened (**Table S1**).

Schistosomes live in the veins surrounding the host intestines, and attach to the vascular endothelium to avoid being swept away in the blood and trapped in host organs. Under *in vitro* culture conditions healthy parasites attach to the substrate with a combination of their oral and ventral suckers (**Movie S1**). We thus reasoned that substrate attachment would be a useful quantitative metric to define RNAi treatments that

affect parasite vitality and predict *in vivo* survival. Therefore, we monitored parasites for 30 days to identify substrate attachment and other visible defects.

Schistosomes possess adult somatic stem cells (neoblasts) that rejuvenate parasite tissues, including the intestine and tegument (skin)(*2, 3*). The parasites also contain large numbers of proliferative germline stem cells (GSCs) in their reproductive organs(*2*) which are essential for producing eggs; the central driver of parasite-induced pathology *in vivo(4)*. Therefore, we monitored the maintenance of neoblasts and GSCs by labeling parasites with the thymidine analog EdU prior to the conclusion of the experiment (**Fig. 1A**). Due to the variable rate at which the reproductive organs of female worms degenerate during *in vitro* culture(*5*), stem cell proliferation was only monitored in male worms. For genes with RNAi phenotypes uncovered during our screen, we confirmed gene identity by sequencing, and mitigated potential off-target effects by designing an additional dsRNA targeting a non-overlapping gene region or by examining sequence identity of hits with other *S. mansoni* genes (**Fig. S1**). These studies identified 195 genes with fully-penetrant attachment phenotypes of which 121 possessed phenotypes in addition to attachment, including: tissue and intestinal edema (36), head (26) and/or tegument (78) degeneration, muscular hypercontraction (6), and death (36) (**Fig. 1B, Table S2**). RNAi of an additional 66 genes resulted in stem cell maintenance defects but caused no other visible phenotypes (*e.g.,* attachment) suggesting an essential role for stem cell maintenance (**Fig. S2, Table S3**). We cannot rule out the possibility of false negatives among the genes with no phenotype and encourage greater scrutiny of such genes by alternate knockdown approaches or analysis of different phenotypic readouts.

Of the 66 genes required for stem cell survival, RNAi of over 90% (60/66) led to defects in the maintenance of both proliferative cells in the male testes and neoblasts (**Fig. S2**). However, for a minority of genes this maintenance defect appeared to be specific to either proliferative cells in the testes or the neoblasts (**Fig. S2**). Gene Ontology enrichment analysis identified genes important for protein translation, including gene products involved in ribosomal structure, tRNA aminoacylation, and rRNA processing as

putative regulators of proliferative cell maintenance (**Fig. S3A**). Although this could reflect an enhanced sensitivity of actively proliferating cells to alterations in protein translation, studies have highlighted "non-housekeeping" roles for translational regulators in controlling stem cell function(*6*).

Of the 195 genes essential for parasite attachment, a large fraction share sequence similarity with other organisms, including other medically-relevant schistosome species (**Table S4**). Additionally, most genes with an attachment phenotype (172/195 genes; 88%) possess a close homolog from *C. elegans* or *D. melanogaster* that likewise has a loss-of-function phenotype (**Table S5**). Gene Ontology analyses of genes with attachment phenotypes further revealed that the dominant group of enriched genes were those encoding components necessary for protein turnover via the ubiquitin-proteasome system (UPS) (**Fig. S3B**). Proteolysis is important for larval and adult viability *in vitro(7, 8)* and our data identified that key components from virtually every arm of the UPS were required for adult parasite vitality during *in vitro* culture (**Fig. S4A**). Indeed, RNAi of nearly all of UPS components resulted in extensive tissue degeneration and in some cases adult parasite death (**Fig. S4B-C**).

To determine if any genes associated with attachment phenotypes encoded proteins targeted by existing pharmacological agents, we searched the literature and the ChEMBL database(*9*) (**Table S6**). This analysis uncovered 205 compounds potentially targeting 49 *S. mansoni* proteins. We selected 14 of these compounds (**Table S7**) and examined the activities of these compounds on worms cultured *in vitro* either by automated worm movement tracking or parasite attachment. More than half of the compounds tested (8/14) on worms at 10 μM reduced parasite movement >75% and half of the compounds (7/14) caused fully-penetrant substrate attachment defects by D7 post-treatment (**Fig. 2A-B, Movie S2**). Similarly, 7 of these compounds affected the movement of post-infective larvae (schistosomula), suggesting activity against multiple life-cycle stages (**Table S8**).

Among the compounds that emerged from these studies was simvastatin, an HMG-CoA reductase inhibitor, with known effects on parasites both *in vitro* and *in vivo(10)*. The proteasome inhibitor ixazomib affected both schistosome movement (**Fig. 2A**) and attachment (**Fig. 2B**), mirroring a recent report using the proteasome inhibitor bortezomib (*7*). However, the most potent effects on adult parasites were observed with CB-5083 and NMS-873 that inhibit the UPS component p97 by either competing with ATP (*11*) or binding to an allosteric site(*12*), respectively (**Fig. S5A**). Similar to the death observed following long-term *p97* RNAi treatment (**Fig. 1B**), both p97 inhibitors led to death *in vitro* (**Movie S3**). Despite their distinct biochemical mechanisms of action, we noted similar deformations in the structure of the parasite tegument following treatment with either CB-5083 or NMS-873, suggesting that these compounds have similar pharmacological effects on the parasite (**Fig. 2C**).

We then assessed if NMS-873 and CB-5083 affected UPS function by measuring the accumulation of ubiquitinated proteins using an antibody that recognizes K48 polyubiquitinated proteins marked for proteasome-mediated destruction(*13*). We observed the accumulation of polyubiquitinated proteins following RNAi of *p97* and after treatment of schistosomes with either CB-5083 or NMS-873 (**Fig. S5B**). Consistent with CB-5083 or NMS-873 acting via *p97* inhibition to blunt protein degradation, we found that *p97* RNAi-treatment together with low concentrations of either drug led to additive increases in polyubiquitinated protein accumulation (**Fig. S5C**). We also observed accumulation of polyubiquitinated proteins following either RNAi of *proteasome subunit beta type-2* or treatment with ixazomib (**Fig. S5D**). These effects on the degradation of ubiquitinated proteins appeared to be specific to inhibition of UPS function, rather than a non-specific effect due to reduced worm vitality (**Fig. S5D**).

We then depleted UPS components using RNAi and surgically transplanted these worms into the mesenteric veins of recipient mice (**Fig. S6A**) and measured parasite egg deposition in host tissues and parasite survival. Following hepatic portal perfusion, we recovered about 55% of transplanted control RNAi-treated worms (**Figs. 2D, S6B**) and these parasites established patent infections, depositing large

number of eggs into the livers of recipient mice (**Figs. 2E, S6C-D**). In contrast, we failed to recover parasites following hepatic portal perfusion from mice receiving *p97* (**Fig. 2D**) or *proteasome subunit beta type-2* (**Fig. S6B).** As a consequence, the livers in these mice were devoid of eggs and we observed no signs of egg-induced granulomas (**Figs. 2E, S6C-D**). We also observed RNAi-treated parasites at various stages of infiltration by host immune cells (**Fig. S6E-F**). This suggests that these parasites are unable to remain in the portal vasculature and are cleared via the liver by the immune system. Taken together, these data highlight the essentially and druggability of the schistosome UPS.

Another group of potentially druggable targets to emerge from our RNAi screen were protein kinases, 19 of which led to defects in either parasite attachment or stem cell maintenance. RNAi of two STE20 serine-threonine kinases: *tao* and *stk25,* which are homologs of the human TAO1/2/3 and STK25/YSK1 protein kinases, respectively, led to rapid detachment from the substrate (**Fig. S7A**) and a concomitant posterior paralysis and hypercontraction of the body, such that the parasites took on a distinctive banana-shaped morphology (**Figs. 3A, S7B, Movie S4**). Aside from RNAi of *stk25* and *tao,* this banana-shaped phenotype of worms was unique, only observed following RNAi of a CCM3/PDCD10 homolog (Smp_031950), a known heterodimerization partner with the mammalian STK25 kinase(*14*). We failed to observe death of either *stk25*- or *tao*- depleted parasites during *in vitro* culture. However, following surgical transplantation, we noted a reduction in the recovery of *tao* or *stk25* RNAi-treated parasites from recipient mice and these recipient mice displayed few signs of egg-induced granuloma formation (**Figs. 3B-C, S7C-D**). Thus, both *tao* and *stk25* appear to be essential for schistosome survival *in vivo*.

Given the unique and specific nature of the *stk25* and *tao* associated "banana" phenotype we reasoned that these kinases may be acting in concert to mediate signaling processes in the worm. The *Drosophila* STK25 ortholog (GCK3) is a substrate of TAO and these proteins function in a signaling cascade essential for tracheal development(*15*). Likewise we observed that recombinant *S. mansoni* STK25 (SmSTK25) could serve as a substrate for the *S. mansoni* TAO (SmTAO) in an *in vitro* kinase assay (**Fig.**

S8A-B). The human STK25 is activated by phosphorylation of a conserved threonine residue within its activation loop(*16*). By mass spectrometry we observed that this conserved threonine within the predicted SmSTK25 activation loop (T^{173}) was phosphorylated following incubation of recombinant SmTAO with catalytically inactive SmSTK25 (**Fig. S8C-D**). Using an antibody that recognizes activation loop phosphorylation in STK25 orthologs(*16*), western blotting revealed SmSTK25 T^{173} autophosphorylation following an *in vitro* kinase reaction; this signal was abrogated in controls lacking ATP and when the SmSTK25 catalytic K^{48} residue was mutated to R (**Figs. 3D, S8E**). Consistent with our mass spectrometry results, we detected robust phosphorylation of T^{173} when recombinant SmTAO was incubated with kinase dead SmSTK25 (**Fig. 3D**), suggesting that SmTAO can phosphorylate a key residue for the activation of the mammalian STK25.

We reasoned that the schistosome TAO and STK25 might be acting in a signaling module to mediate critical processes in the parasite. To define these processes, we performed transcriptional profiling on RNAi-treated parasites just prior to observing detachment and hypercontraction (Day 6 and Day 9 for *tao* and *stk25* RNAi treatments, respectively) (**Fig. S9A-B**). We found that expression of differentially regulated genes following RNAi of either *tao* or *stk25* were correlated (**Fig. 3E**) and that more than half of these differentially regulated genes were common in both datasets (**Fig. S9C, Table S9**). Importantly, RNAi of either *tao* or *stk25* was specific, not affecting expression of the other kinase gene of this pair (**Fig. 3E-F**).

Examining the tissue-specific expression of differentially-regulated genes on an adult schistosome single cell expression atlas using cells from schistosome somatic tissues(*17*), we found that roughly 40% (51/129) of the most down-regulated genes following *tao* and *stk25* RNAi were specific markers of parasite muscle cells (**Fig. S10A-C, Table S9**). Indeed, nearly half of all mRNAs specifically-enriched in muscle cells (60/135) from this single cell atlas, including key muscle contractile proteins, were down-regulated

following RNAi of both *tao* and *stk25* (**Figs. 3F, S10B, D, Table S10**). Importantly, these transcriptional effects appeared to be largely specific to parasite muscles (**Figs. 3F, S10B, Table S10**).

In principle, loss of muscle-specific mRNAs could be due to either loss of muscle cells or down-regulation of muscle-specific mRNAs. We thus labeled F-actin in schistosome muscle fibers with phalloidin and performed *in situ* hybridization to detect muscle-specific mRNAs. RNAi-treated parasites exhibited a reduction in the expression of mRNAs encoding the contractile proteins Tropomyosin 1 and a Myosin Light Chain by *in situ* hybridization (**Fig. 3G**), but no qualitative defects in phalloidin staining of body wall muscles (**Fig. S11**). Thus, it appears that these kinases are required to maintain the transcription of many muscle-specific mRNAs in intact muscle cells. Interestingly, the heads of *tao* and *stk25* RNAi parasites retained their capacity for movement (**Movie S4**) and partially maintained the expression of muscle-specific mRNAs (**Fig. 3G**). Thus, there appears to be a relationship between the maintenance of muscle-specific mRNA expression and locomotion.

Taken in their entirety, our data suggest that STK25 and TAO kinases cooperate in the schistosome to mediate signaling essential for sustaining the transcription of muscle-specific mRNAs. As a consequence, loss of either SmSTK25 or SmTAO activity results in muscular function defects compromising parasite survival *in vivo*. As whole-body knockouts of mouse STK25 are homozygous viable displaying no obvious deleterious phenotypes(*18*), SmSTK25 represents an attractive target for therapeutic intervention. Similar cross-examination of genes associated with other phenotypic classes (*e.g.,* tissue edema) may provide insights into the specificity of the various phenotypes observed in this work.

Technological advances have paved the way for large-scale analyses of gene function in protozoan parasites(*19-21*), but, have been lacking in helminth parasites. Our systematic analysis of gene function in schistosomes allowed us to effectively prioritize targets and potential specific inhibitors with activities on worms. Future efforts should not only further explore the potency and selectivity of compounds our studies have uncovered (**Fig. 2A-B, Table S6)**, but larger libraries of compounds with known molecular targets

(*22*). However, to mitigate potential issues with host toxicity it is also worth exploring whether parasite-selective inhibitors of validated target proteins can be uncovered. Not only does this study enhance our understanding of schistosome biology, it provides a new lens to prioritize genes of interest in other medically- and agriculturally-important parasitic flatworms. Collectively, we anticipate this study will expedite the discovery of new anti-helminthics.

References

1. A. Guidi *et al.*, Application of RNAi to Genomic Drug Target Validation in Schistosomes. *PLoS Negl Trop Dis* **9**, e0003801 (2015).

2. J. J. Collins, III *et al.*, Adult somatic stem cells in the human parasite *Schistosoma mansoni*. *Nature* **494**, 476-479 (2013).

3. J. J. Collins, III, G. R. Wendt, H. Iyer, P. A. Newmark, Stem cell progeny contribute to the schistosome host-parasite interface. *Elife* **5**, (2016).

4. E. J. Pearce, A. S. MacDonald, The immunobiology of schistosomiasis. *Nat Rev Immunol* **2**, 499-511 (2002).

5. J. Wang, R. Chen, J. J. Collins, III, Systematically improved in vitro culture conditions reveal new insights into the reproductive biology of the human parasite *Schistosoma mansoni*. *PLoS Biol* **17**, e3000254 (2019).

6. M. Buszczak, R. A. Signer, S. J. Morrison, Cellular differences in protein synthesis regulate tissue homeostasis. *Cell* **159**, 242-251 (2014).

7. B. Bibo-Verdugo *et al.*, The Proteasome as a Drug Target in the Metazoan Pathogen, *Schistosoma mansoni*. *ACS Infect Dis*, (2019).

8. J. F. Nabhan, F. El-Shehabi, N. Patocka, P. Ribeiro, The 26S proteasome in *Schistosoma mansoni*: bioinformatics analysis, developmental expression, and RNA interference (RNAi) studies. *Exp Parasitol* **117**, 337-347 (2007).

9. D. Mendez *et al.*, ChEMBL: towards direct deposition of bioassay data. *Nucleic Acids Res* **47**, D930-D940 (2019).

10. L. Rojo-Arreola *et al.*, Chemical and genetic validation of the statin drug target to treat the helminth disease, schistosomiasis. *PLoS One* **9**, e87594 (2014).

11. D. J. Anderson *et al.*, Targeting the AAA ATPase p97 as an Approach to Treat Cancer through Disruption of Protein Homeostasis. *Cancer Cell* **28**, 653-665 (2015).

12. P. Magnaghi *et al.*, Covalent and allosteric inhibitors of the ATPase VCP/p97 induce cancer cell death. *Nat Chem Biol* **9**, 548-556 (2013).

13. K. Newton *et al.*, Ubiquitin chain editing revealed by polyubiquitin linkage-specific antibodies. *Cell* **134**, 668-678 (2008).

14. D. F. Ceccarelli *et al.*, CCM3/PDCD10 heterodimerizes with germinal center kinase III (GCKIII) proteins using a mechanism analogous to CCM3 homodimerization. *J Biol Chem* **286**, 25056-25064 (2011).

15. C. L. C. Poon *et al.*, A Hippo-like Signaling Pathway Controls Tracheal Morphogenesis in *Drosophila melanogaster*. *Dev Cell* **47**, 564-575 e565 (2018).

16. C. Preisinger *et al.*, YSK1 is activated by the Golgi matrix protein GM130 and plays a role in cell migration through its substrate 14-3-3zeta. *J Cell Biol* **164**, 1009-1020 (2004).

17. G. R. Wendt *et al.*, A single-cell RNAseq atlas of the pathogenic stage of *Schistosoma mansoni* identifies a key regulator of blood feeding. *bioRxiv*, (2020).

18. M. Amrutkar *et al.*, Genetic Disruption of Protein Kinase STK25 Ameliorates Metabolic Defects in a Diet-Induced Type 2 Diabetes Model. *Diabetes* **64**, 2791-2804 (2015).

19. S. Alsford *et al.*, High-throughput phenotyping using parallel sequencing of RNA interference targets in the African trypanosome. *Genome Res* **21**, 915-924 (2011).

20. E. Bushell *et al.*, Functional Profiling of a *Plasmodium* Genome Reveals an Abundance of Essential Genes. *Cell* **170**, 260-272 e268 (2017).

21. S. M. Sidik *et al.*, A Genome-wide CRISPR Screen in *Toxoplasma* Identifies Essential Apicomplexan Genes. *Cell* **166**, 1423-1435 e1412 (2016).

22. J. Janes *et al.*, The ReFRAME library as a comprehensive drug repurposing library and its application to the treatment of cryptosporidiosis. *Proc Natl Acad Sci U S A* **115**, 10750-10755 (2018).

23. P. F. Basch, Cultivation of *Schistosoma mansoni* in vitro. I. Establishment of cultures from cercariae and development until pairing. *J Parasitol* **67**, 179-185 (1981).

24. J. J. Collins, III *et al.*, Genome-Wide Analyses Reveal a Role for Peptide Hormones in Planarian Germline Development. *PLoS Biol* **8**, e1000509 (2010).

25. J. J. Collins, III, R. S. King, A. Cogswell, D. L. Williams, P. A. Newmark, An atlas for *Schistosoma mansoni* organs and life-cycle stages using cell type-specific markers and confocal microscopy. *PLoS Negl Trop Dis* **5**, e1009 (2011).

26. J. Schindelin *et al.*, Fiji: an open-source platform for biological-image analysis. *Nat Methods* **9**, 676-682 (2012).

27. J. N. Collins, J. J. Collins, III, Tissue Degeneration following Loss of *Schistosoma mansoni cbp1* Is Associated with Increased Stem Cell Proliferation and Parasite Death In Vivo. *PLoS Pathog* **12**, e1005963 (2016).

28. International Helminth Genomes Consortium, Comparative genomics of the major parasitic worms. *Nat Genet* **51**, 163-174 (2019).

29. S. D. Lamore *et al.*, Deconvoluting Kinase Inhibitor Induced Cardiotoxicity. *Toxicol Sci* **158**, 213-226 (2017).

30. J. J. Lynch, 3rd, T. R. Van Vleet, S. W. Mittelstadt, E. A. G. Blomme, Potential functional and pathological side effects related to off-target pharmacological activity. *J Pharmacol Toxicol Methods* **87**, 108-126 (2017).

31. J. Bowes *et al.*, Reducing safety-related drug attrition: the use of in vitro pharmacological profiling. *Nat Rev Drug Discov* **11**, 909-922 (2012).

32. K. C. L. Whatley *et al.*, The repositioning of epigenetic probes/inhibitors identifies new anti-schistosomal lead compounds and chemotherapeutic targets. *PLoS Negl Trop Dis* **13**, e0007693 (2019).

33. C. Marcellino *et al.*, WormAssay: a novel computer application for whole-plate motion-based screening of macroscopic parasites. *PLoS Negl Trop Dis* **6**, e1494 (2012).

34. H. L. Whiteland *et al.*, An Abies procera-derived tetracyclic triterpene containing a steroid-like nucleus core and a lactone side chain attenuates in vitro survival of both Fasciola hepatica and Schistosoma mansoni. *Int J Parasitol Drugs Drug Resist* **8**, 465-474 (2018).

35. G. R. Wendt *et al.*, Flatworm-specific transcriptional regulators promote the specification of tegumental progenitors in *Schistosoma mansoni*. *Elife* **7**, (2018).

36. T. Stuart *et al.*, Comprehensive Integration of Single-Cell Data. *Cell* **177**, 1888-1902 e1821 (2019).

37. D. C. Trudgian, H. Mirzaei, Cloud CPFP: a shotgun proteomics data analysis pipeline using cloud and high performance computing. *J Proteome Res* **11**, 6282-6290 (2012).

38. D. C. Trudgian *et al.*, CPFP: a central proteomics facilities pipeline. *Bioinformatics* **26**, 1131-1132 (2010).

39. R. Craig, R. C. Beavis, TANDEM: matching proteins with tandem mass spectra. *Bioinformatics* **20**, 1466-1467 (2004).

40. L. Y. Geer *et al.*, Open mass spectrometry search algorithm. *Journal of proteome research* **3**, 958-964 (2004).

41. J. E. Elias, S. P. Gygi, Target-decoy search strategy for increased confidence in large-scale protein identifications by mass spectrometry. *Nature methods* **4**, 207-214 (2007).

42. D. C. Trudgian, R. Singleton, M. E. Cockman, P. J. Ratcliffe, B. M. Kessler, ModLS: post-translational modification localization scoring with automatic specificity expansion. *J. Proteomics Bioinform* **5**, 283-289 (2012).

43. B. J. Bolt *et al.*, Using WormBase ParaSite: An Integrated Platform for Exploring Helminth Genomic Data. *Methods Mol Biol* **1757**, 471-491 (2018).

44. A. Rozanski *et al.*, PlanMine 3.0-improvements to a mineable resource of flatworm biology and biodiversity. *Nucleic Acids Res* **47**, D812-D820 (2019).

45. T. W. Harris *et al.*, WormBase: a modern Model Organism Information Resource. *Nucleic Acids Res* **48**, D762-D767 (2020).

46. J. Thurmond *et al.*, FlyBase 2.0: the next generation. *Nucleic Acids Res* **47**, D759-D765 (2019).

47. H. J. Zhou *et al.*, Discovery of a First-in-Class, Potent, Selective, and Orally Bioavailable Inhibitor of the p97 AAA ATPase (CB-5083). *J Med Chem* **58**, 9480-9497 (2015).

48. E. Kupperman *et al.*, Evaluation of the proteasome inhibitor MLN9708 in preclinical models of human cancer. *Cancer Res* **70**, 1970-1980 (2010).

49. M. Treiman, C. Caspersen, S. B. Christensen, A tool coming of age: thapsigargin as an inhibitor of sarco-endoplasmic reticulum Ca(2+)-ATPases. *Trends Pharmacol Sci* **19**, 131-135 (1998).

50. E. E. Slater, J. S. MacDonald, Mechanism of action and biological profile of HMG CoA reductase inhibitors. A new therapeutic alternative. *Drugs* **36 Suppl 3**, 72-82 (1988).

51. A. Scuto *et al.*, The novel histone deacetylase inhibitor, LBH589, induces expression of DNA damage response genes and apoptosis in Ph- acute lymphoblastic leukemia cells. *Blood* **111**, 5093-5100 (2008).

52. J. Arts *et al.*, JNJ-26481585, a novel "second-generation" oral histone deacetylase inhibitor, shows broad-spectrum preclinical antitumoral activity. *Clin Cancer Res* **15**, 6841-6851 (2009).

53. K. Lundgren *et al.*, BIIB021, an orally available, fully synthetic small-molecule inhibitor of the heat shock protein Hsp90. *Mol Cancer Ther* **8**, 921-929 (2009).

54. D. L. Menezes *et al.*, The novel oral Hsp90 inhibitor NVP-HSP990 exhibits potent and broad-spectrum antitumor activities in vitro and in vivo. *Mol Cancer Ther* **11**, 730-739 (2012).

55. T. Maes *et al.*, ORY-1001, a Potent and Selective Covalent KDM1A Inhibitor, for the Treatment of Acute Leukemia. *Cancer Cell* **33**, 495-511 e412 (2018).

56. G. Caceres *et al.*, Determination of chemotherapeutic activity in vivo by luminescent imaging of luciferase-transfected human tumors. *Anticancer Drugs* **14**, 569-574 (2003).

57. L. M. Lasko *et al.*, Discovery of a selective catalytic p300/CBP inhibitor that targets lineage-specific tumours. *Nature* **550**, 128-132 (2017).

58. C. H. Jin *et al.*, Discovery of N-((4-([1,2,4]triazolo[1,5-a]pyridin-6-yl)-5-(6-methylpyridin-2-yl)-1H-imidazol-2 -yl)methyl)-2-fluoroaniline (EW-7197): a highly potent, selective, and orally bioavailable inhibitor of TGF-beta type I receptor kinase as cancer immunotherapeutic/antifibrotic agent. *J Med Chem* **57**, 4213-4238 (2014).

59. M. Muraki *et al.*, Manipulation of alternative splicing by a newly developed inhibitor of Clks. *J Biol Chem* **279**, 24246-24254 (2004).

Acknowledgements: We thank M. McConathy, C. Furrh, and G. Pagliuca for technical assistance, F. Hunter and N. Bosc for advice about retrieving data from ChEMBL, and M. Cobb and E. Ross for suggestions regarding kinase studies. Infected mice and *B. glabrata* snails were provided by the National Institute of Allergy and Infectious Diseases (NIAID) Schistosomiasis Resource Center of the Biomedical Research Institute (Rockville, MD, USA) through National Institutes of Health (NIH)-NIAID Contract HHSN272201700014I for distribution through BEI Resources. **Author contributions:** Conceptualization, J.W., C.P., M.B., K.F.H., J.J.C.; investigation, J.W., C.P., G.P, A.C., Z.L., I.G., J.N.R.C.; Writing-original draft, J.W., C.P., J.J.C.; writing–review and editing, all authors. **Funding:** The work was supported by the National Institutes of Health R01AI121037 (JJC), the Welch Foundation I-1948-20180324 (JJC), the Burroughs Wellcome Fund (JJC), and the Wellcome Trust 107475/Z/15/Z (JJC/KFH/MB) and 206194 (MB). CP was supported by Howard Hughes Medical Institute Gilliam Fellowship and National Science Foundation Graduate Research Fellowship SPA0001848. **Competing interests:** The authors declare no competing interest. **Data and materials availability:** Videos of RNAi attachment phenotypes can be accessed at www.collinslab.org/schistocyte or at https://doi.org/10.5061/dryad.zs7h44j4v. RNAseq analyses have been deposited in the NCBI Gene Expression Omnibus GSE146720.

Supplemental Materials

Materials and Methods

Tables S1-S10

Figs S1-S11

References (23-59)

Movies S1-S4

Fig. 1. Summary of RNAi phenotypes.

(A) RNAi treatment regime. Parasites were monitored for visible abnormalities and at D29 EdU was added to media to label proliferative cells. **(B**) Categories of RNAi phenotypes observed. *kin-17* (Smp_023250), *cog1* (Smp_132980), *p97* (Smp_018240), *c44* (Smp_136260), *prpf4b* (Smp_068960), *gtf2f1* (Smp_088460), *stk25* (Smp_096640). Scale bar: 100 μm

Fig. 2. Compounds prioritized from RNAi studies have effects on schistosomes *in vitro.*

(A) Compounds (red text) predicted to target schistosome proteins (blue text) essential for parasite attachment at 10 μM for their effects on worm motility. n = 12 worm pairs, n = 3 biological replicates; data are mean +/- SD. Dashed line, threshold for 75% reduction in motility **(B)** Heatmap showing time course measuring the fraction of male worms attached to the substrate following treatment with compounds for 72 hours as in **A**. n = 3 biological replicates **(C)** Effects of CB-5083 or NMS-873 (10 μM, 72 hrs) treatment on male parasites. **(D**) Percent recovery *p97*(RNAi) or control(RNAi) male parasites surgically transplanted into mice. n = 8 transplants for each group. ****, $p < 0.0001$, t-test**;** data are mean +/- 95% CI**. (E)** Hematoxylin and Eosin staining of livers from mice receiving control or *p97(RNAi)* parasites. Egg-induced granulomas (yellow arrows). (top right) counts of eggs/cm liver section are shown, counts from sections from n = 3 livers. Scale bars: C, E, 100 μm.

Fig. 3. The protein kinases SmSTK25 and SmTAO are essential to maintain muscular function

(A) RNAi of *stk25* or *tao* causes parasite hypercontraction. (**B-C**) Percent recovery *stk25*(RNAi), *tao*(RNAi), or control(RNAi) male parasites surgically transplanted into mice. n $\geq$ 11 transplants for each group. ****, $p < 0.0001$, t-test; data are mean +/- 95% CI. **(D)** Western blot to detect phospho-T173 (p-SmSTK25) or total SmSTK25 following an *in vitro* kinase reaction +/- ATP. kinase dead SmTAO(kdSmTAO). Representative of n = 2 experiments. **(E)** Scatter plot showing the relationship between the differentially expressed genes ($p\ adj < 0.001$, Benjamini-Hochberg corrected Wald test) following *stk25* or *tao* RNAi-treatment ($r = 0.9$, $p < 0.0001$, Pearson correlation). **(F)** Heatmap showing expression of tissue-specific transcripts following RNAi of *tao* or *stk25*. **(G)**. *in situ* hybridization for *tropomyosin 1* (*tpm1,* Smp_340760) and a myosin light chain (*myl2,* Smp_132670) following RNAi at D13. Scale bars: A, 500 μm; G, 100 μm.

Fig. 1

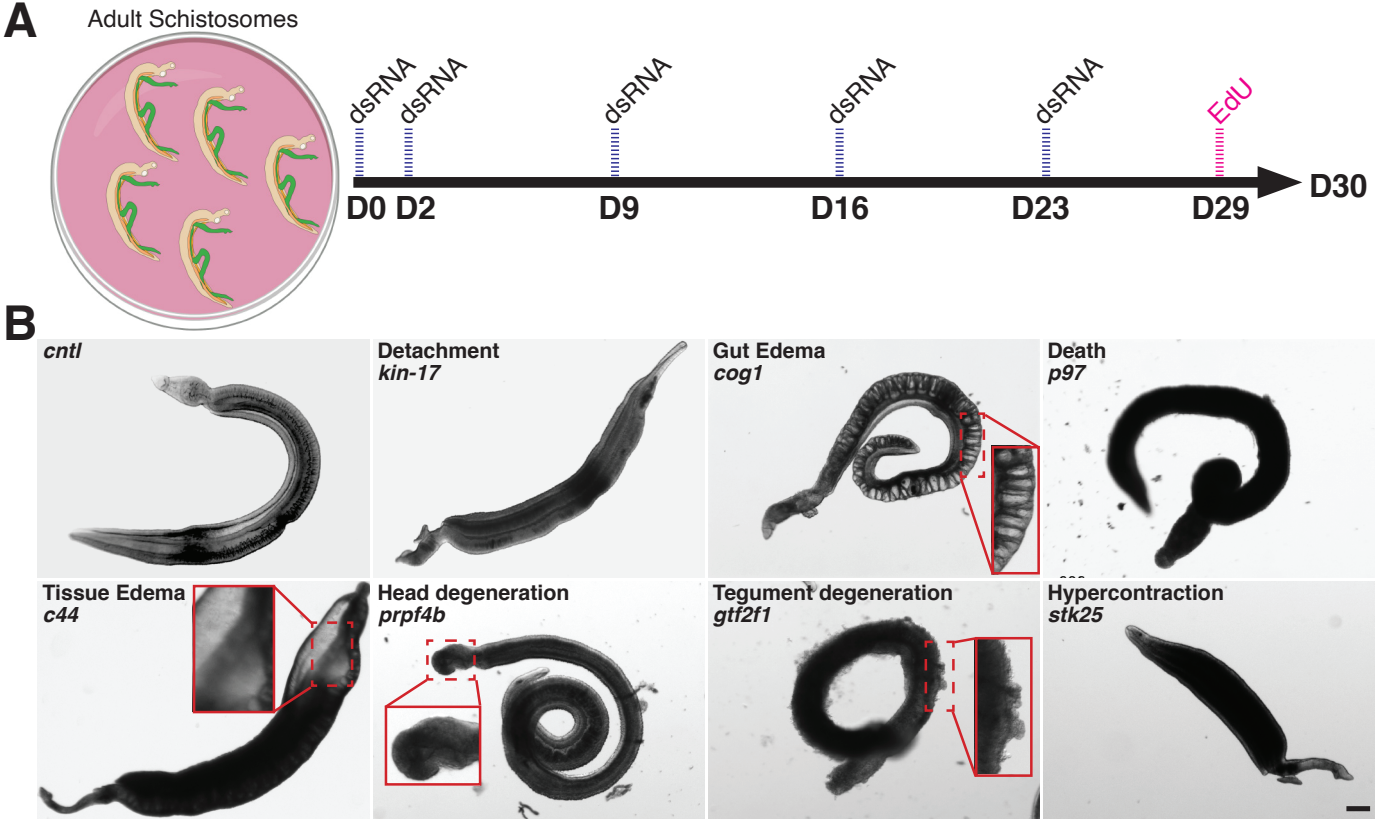
A
Adult Schistosomes
dsRNA
dsRNA
dsRNA
dsRNA
dsRNA
EdU
D0 D2
D9
D16
D23
D29
D30
B
cntl
Detachment
kin-17
Gut Edema
cog1
Death
p97
Tissue Edema
c44
Head degeneration
prpf4b
Tegument degeneration
gtf2f1
Hypercontraction
stk25

Fig. 2

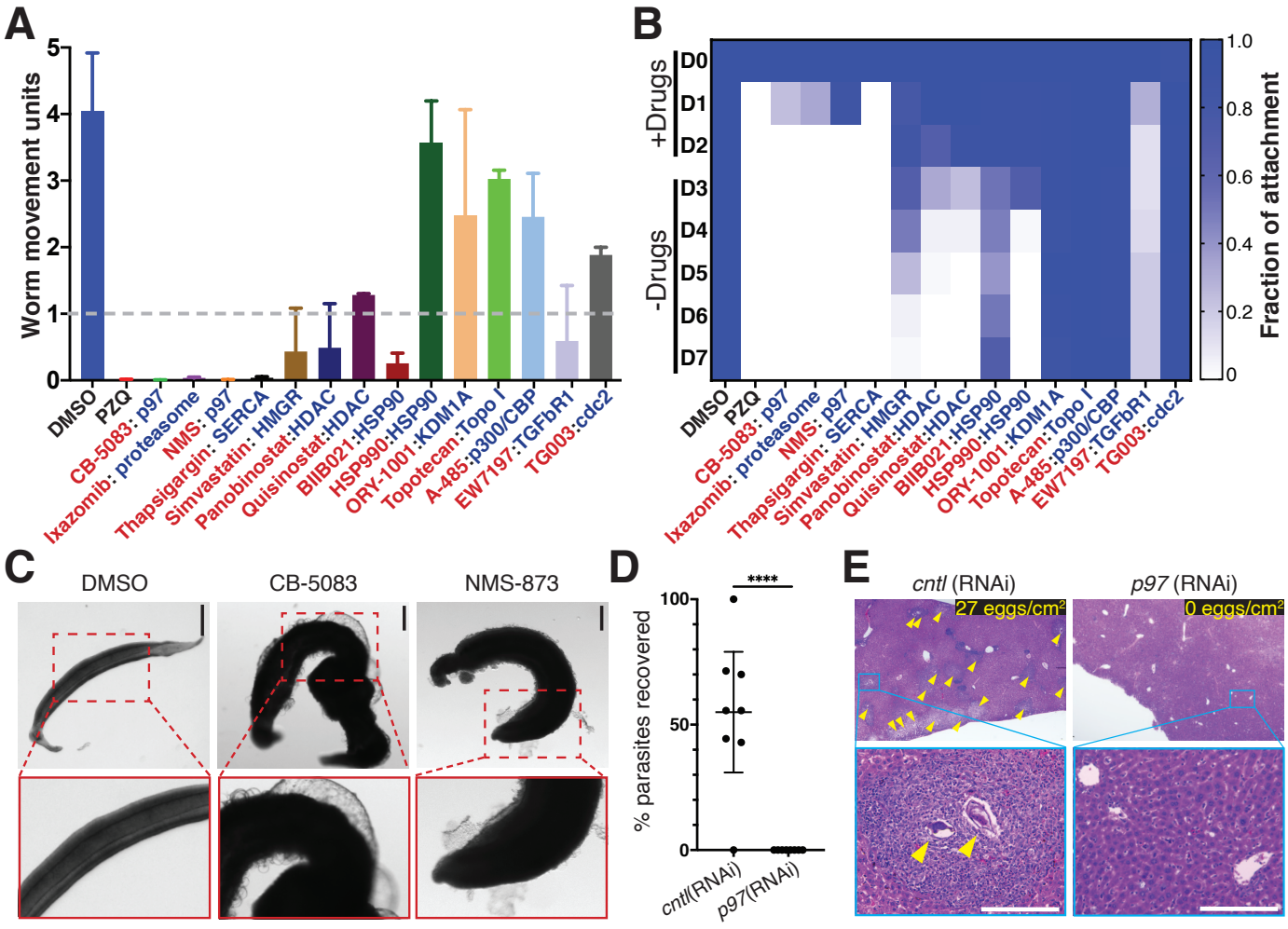
A
Worm movement units
0
1
2
3
4
5
DMSO
PZQ
CB-5083: p97
Ixazomib: proteasome
NMS: p97
Thapsigargin: SERCA
Simvastatin: HMGR
Panobinostat:HDAC
Quisinostat:HDAC
BIIB021:HSP90
HSP990:HSP90
ORY-1001:KDM1A
Topotecan:Topo I
A-485:p300/CBP
EW7197:TGFbR1
TG003:cdc2
B
+Drugs
-Drugs
D0
D1
D2
D3
D4
D5
D6
D7
Fraction of attachment
0
0.2
0.4
0.6
0.8
1.0
C
DMSO
CB-5083
NMS-873
D
% parasites recovered
****
100
50
0
cntl(RNAi)
p97(RNAi)
E
cntl (RNAi)
p97 (RNAi)
27 eggs/cm²
0 eggs/cm²

Fig. 3

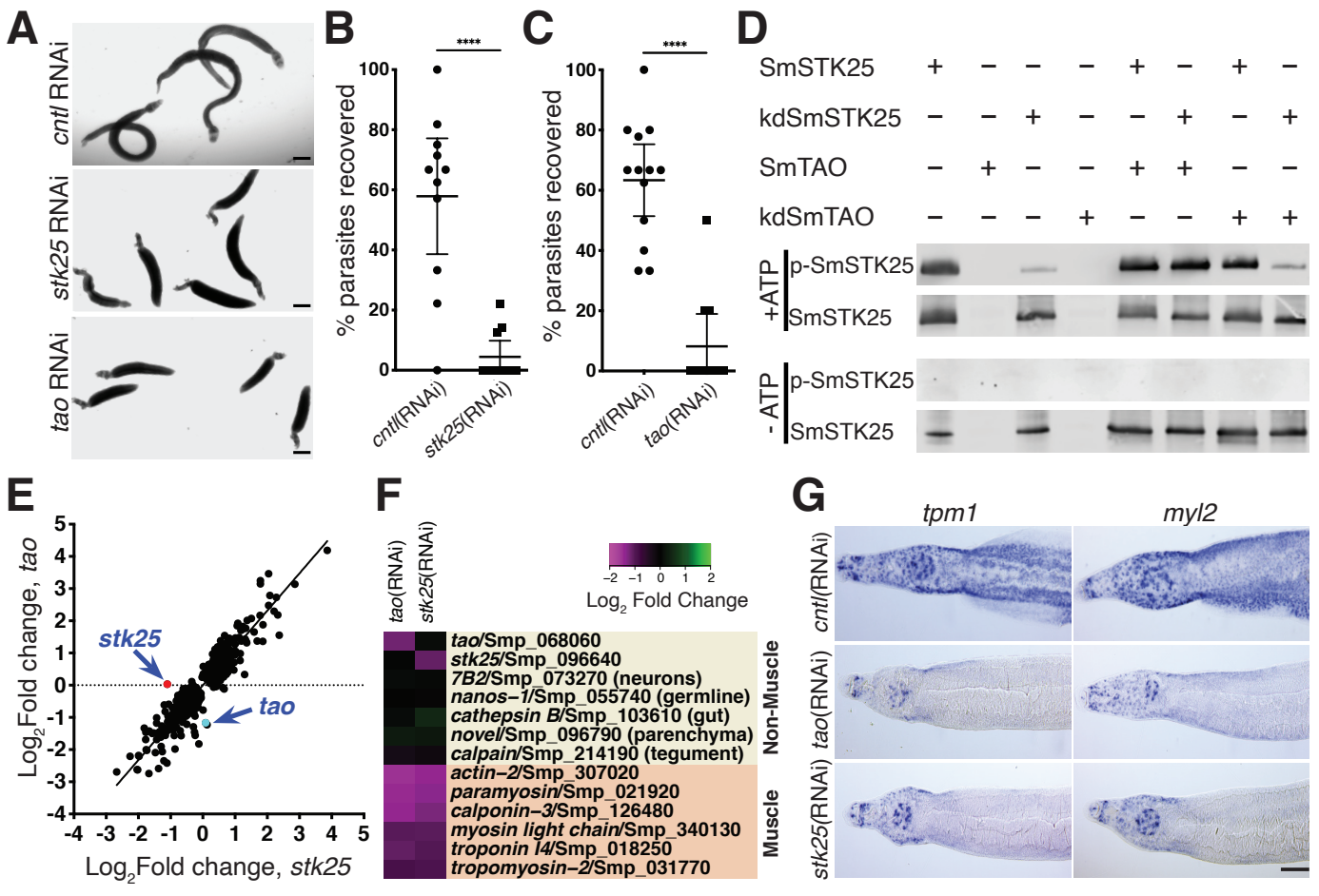
A
cntl RNAi
stk25 RNAi
tao RNAi
B
% parasites recovered
****
cntl(RNAi)
stk25(RNAi)
C
% parasites recovered
****
cntl(RNAi)
tao(RNAi)
D
SmSTK25
kdSmSTK25
SmTAO
kdSmTAO
+ATP
p-SmSTK25
SmSTK25
- ATP
p-SmSTK25
SmSTK25
E
Log2Fold change, tao
Log2Fold change, stk25
stk25
tao
F
tao(RNAi)
stk25(RNAi)
Log2 Fold Change
tao/Smp_068060
stk25/Smp_096640
7B2/Smp_073270 (neurons)
nanos–1/Smp_055740 (germline)
cathepsin B/Smp_103610 (gut)
novel/Smp_096790 (parenchyma)
calpain/Smp_214190 (tegument)
Non-Muscle
actin–2/Smp_307020
paramyosin/Smp_021920
calponin–3/Smp_126480
myosin light chain/Smp_340130
troponin I4/Smp_018250
tropomyosin–2/Smp_031770
Muscle
G
tpm1
myl2
cntl(RNAi)
tao(RNAi)
stk25(RNAi)

Science
AAAS

Supplementary Materials for

Large-scale RNAi screening uncovers therapeutic targets in the parasite *Schistosoma mansoni*

Jipeng Wang, Carlos Paz, Gilda Padalino, Avril Coghlan, Zhigang Lu, Irina Gradinaru, Julie N.R. Collins, Matthew Berriman, Karl F. Hoffmann, James J. Collins III*
Correspondence to: JamesJ.Collins@UTSouthwestern.edu

This PDF file includes:

Other Supplementary Materials for this manuscript include the following:

Materials and Methods

Parasites

Adult *S. mansoni* (NMRI strain) (6–7 weeks post-infection) or juvenile worms (4–5 weeks post-infection) were harvested from infected female Swiss Webster mice by hepatic portal vein perfusion with 37°C DMEM (Mediatech, Manassas, VA) plus 8% Horse Serum and heparin. Parasites were rinsed in DMEM + plus 8% Horse Serum and cultured (37°C/5% CO_2) in Basch's Medium 169(*23*) and 1× Antibiotic-Antimycotic (Gibco/Life Technologies, Carlsbad, CA 92008). Experiments with and care of vertebrate animals were performed in accordance with protocols approved by the Institutional Animal Care and Use Committee (IACUC) of UT Southwestern Medical Center (approval APN: 2017-102092).

RNAi screen

For our screen we prioritized genes that were expressed in adult male schistosome somatic tissues (using an existing expression dataset (*3*)). This prioritized list included genes encoding enzymes, cell-surface receptors, ion channels, to enrich for proteins with potential druggability, and hypothetical proteins of unknown function, to ascribe function to these genes. However, early iterations of RNAi screening found that positive PCR products could not be obtained for ~30% of gene models from v5 of the *S. mansoni* genome. To ensure a large fraction of PCRs yielded products we manually curated gene models to define stretches of mRNA sequence supported by experimental data. Using these manually curated stretches of sequence, primers were designed to amplify ~700 bp fragments using BatchPrimer3 http://batchprimer3.bioinformatics.ucdavis.edu/index.html. For gene fragments shorter than 700 bp, primers were designed to cover as much of the transcript as possible. For reverse transcription of double stranded RNAs, a T7 promoter sequence (GAATTTAATACGACTCACTATA) was added to the 5' end of each oligo. To facilitate DNA sequencing of cDNAs associated with RNAi phenotypes, we added a *NotI* or *AscI* restriction enzyme site between the T7 and gene-specific sequences on the forward and reverse oligos, respectively. These oligos were synthesized and packaged in 96-well plates and used for PCR using adult schistosome cDNA as a template. 5 µL of PCR products were then used for *in vitro* transcription to generate dsRNA in 100 µL as previously described (*24*). After overnight incubation at 37 ºC, dsRNAs were annealed by a successive 3-min gradient incubation at 95 ºC, 75 ºC, and 55 ºC, then cooled down at room temperature for 5 min. The presence and size of PCR products and dsRNA were all analyzed by agarose gel electrophoresis and samples stored at -20 ºC. For RNAi treatments, approximately 5 pairs of adult parasites were placed in 3 mL Basch 169 media in a 12-well plate and treated with 20 µL dsRNA at D0, D2, D9, D16 and D23. To examine cell proliferation, the media were supplemented with EdU (10 µM) at D29. On day 30, videos were captured for RNAi treatments that caused visible RNAi phenotypes and after video acquisition all parasites were fixed and processed for EdU detection (*2*). During the entire 30D RNAi treatment regime, media was changed every 1-2 days and worm attachment and morphological changes were monitored.

To validate the identity of hits from the initial RNAi screening, the original PCR products were digested with NotI (NEB) for 30 min at 37 ºC, gel purified (Zymoclean Gel DNA Recovery Kit), and sequenced with a T7 primer. Sequences of genes validated by sequencing were uploaded into BatchPrimer3 to design new primers that amplify a fragment sharing no overlap with the PCR products from the initial RNAi screening. In cases where genes sequences were too short to design non-overlapping amplicons, we retained the original primer sequences. These primers were synthesized without further modification, used to generate PCR products, and then inserted into pJC53.2 using TA cloning (*24*). These plasmids were purified from *E. coli*, validated by sequencing, and used as a template to generate dsRNA. We then repeated the RNAi treatment regime used in the original screen. In order to be considered a hit a gene had to display a similar and fully-penetrant phenotype in at least three independent experiments conducted on separate days from different liver perfusions using distinct batches of dsRNA.

Parasite labelling and imaging

Whole-mount in situ hybridization (*3*), EdU detection (*2*), and phalloidin staining (*25*) were performed as previously described. For in situ hybridization, riboprobes were generated from cDNA fragments amplified using primers for tropomyosin-1 (Smp_340760, gagaaagagaatgctatggaaagagc/cctcattttgtagtttagatacttgacg) or myosin light chain (Smp_132670, gttgctctgtgttaagttaacatggg/gttagtcctaaatgtcttgattgcc). Brightfield images of in situ hybridizations and worm morphology/movement were imaged using a Zeiss AxioZoom V16 (Zeiss, Germany) equipped with a transmitted light base and a Zeiss AxioCam 105 Color camera. Fluorescent images were acquired using a Nikon A1+ laser scanning confocal microscope. For worm length quantification, phalloidin-stained male worms (13 days post-RNAi) were imaged and worm length measured using NIH ImageJ, Fiji distribution (*26*).

Transplantation of dsRNA-treated Schistosomes

Parasites 4–5 weeks post-infection were recovered from mice and treated with 30 μg/mL dsRNA for 4 days in Basch Media 169 with a daily replacement of media and dsRNA and surgically transplanted into naïve male mice as previously described (*27*). Briefly, 10 pairs of adult worms were loaded into a syringe and injected into the cecal vein of a young male Swiss Webster mice (~25–30 g), then the syringe was flushed to determine how many parasites were injected. On day 26 post-transplantation, mice were sacrificed and perfused to recover parasites. Male and female parasites were counted and livers were removed and fixed for 30–40 hours in 4% formaldehyde in PBS. The percentage of parasite recovery was determined by dividing the number of male worms transplanted by the number of male parasites recovered following perfusion. Livers from individual mice were sectioned and processed for Hematoxylin and Eosin staining by the UT Southwestern Molecular Pathology Core.

Detection of polyubiquitinated proteins by western blot

For RNA interference, 10 single-sex male adult worms (6 weeks post infection) were treated with 30 μg/mL dsRNA in Basch Media 169 for 8 days. Media and dsRNA were changed daily. On day 9, worms were collected and flash frozen. For drug treatment, 10 male adult worms (single or paired with females) were supplemented with either DMSO, NMS-873 or CB-5083. After 24 hrs, male parasites were separated from females using 0.25% tricaine in Basch Media 169 and flash frozen. Male worm samples were homogenized with a pestle in 50 μL lysis buffer containing 2× sample buffer, protease inhibitor cocktail (Roche, cOmplete Mini, EDTA-free Tablets) and 10mM DTT. The lysates were then sonicated on high for 5 min (30 sec on, 30 sec off) using a Bioruptor UCD-200. Lysates were centrifuged for 5 min at 10,000 *g* to remove debris. Total protein was measured using the Detergent Compatible Bradford Assay (Pierce). 35 μg of protein samples denatured in SDS Sample buffer (95°C for 5min) were separated on a Bio-Rad 4-20% TGX Stain-Free gel along with Precision Plus Protein Dual Color Standards (Bio-Rad) as a marker. Proteins were then transferred to a nitrocellulose membrane (Bio-Rad) and confirmed by Ponceau S staining. The membrane was blocked in a 1:5 solution of Li-Cor Odyssey Blocking buffer in PBS for 1hr before being immunoblotted overnight at 4°C with 1:500 K48-linkage Specific Polyubiquitin Antibody (Cell Signaling Technology, 4289S) and 0.01 μg/mL mouse anti-actin antibody (Developmental Studies Hybridoma Bank, JLA20) diluted in a 1:5 solution of Li-Cor Odyssey Blocking buffer in PBS. The membrane was washed 3× in TBST and then incubated in 1:5 Li-Cor Odyssey Blocking buffer containing the secondary antibodies (1:10,000 Li-Cor, 925-68071, goat anti-rabbit IRDye 680 RD, and 1:20,000 Li-Cor, 925-32280, goat anti-mouse IgM IRDye 800CW) for 1hr at RT. The blot was washed in TBST 3× before being imaged on a Li-Cor Odyssey Infrared Imager.

Compound prioritization

To manually search for existing drugs targeting "detachment" hits from our RNAi screen, we performed protein-protein BLAST against the *Homo sapiens* proteome to find the closest human homolog to our RNAi hits. We then manually searched a variety of databases (*e.g.,* GeneCards, Google, DrugBank, Therapeutic Targets Database) and chemical vendors (*e.g.,* Selleckchem) for inhibitors against these human proteins. In each instance, we consulted the published literature to give preference to compounds likely to be selective for a given target. If several such drugs were available, preference was given to those that were also orally

bioavailable and/or FDA approved/in clinical trials. For larger-scale discovery of compounds, the *S. mansoni* protein sequences of genes with 'detachment' phenotypes were used to search the ChEMBL database (*9*), to identify compounds predicted to interact with them. To do this, we followed the protocol previously described (*28*) with the following differences. First, for each *S. mansoni* gene, we identified its top BLASTP hit among all ChEMBL targets, as well as any ChEMBL targets having BLAST hits with *E*-values within 10^5 of the top hit's *E*-value; and then extracted from ChEMBL the drugs/compounds with bioactivities against those particular ChEMBL targets. Second, when calculating the 'toxicology target interaction' component of a compound's score, we checked whether ChEMBL predicted with probability >0.5 that the compound interacts with one of 108 toxicology targets curated from (*29-31*).

Evaluation of effects of compounds on worms

in vitro evaluation of selected compounds (single-point concentrations, 10 μM in 0.1% DMSO) on adult movement was replicated three times using a single worm pair per well (two technical replicates each time, n = 12), as previously described (*32*). Worm pairs co-cultivated with DMSO (0.1% negative control) and Praziquantel (PZQ) (10 μM in 0.1% DMSO; positive control) were included in each experiment. Following incubation at 37˚C for 72 hrs in a humidified atmosphere containing 5% CO_2, a digital image processing-based system was used for the assessment of parasite motility. Both hardware and software components of this system (WormassayGP2) were inspired by the digital macroscopic imaging apparatus previously described (*33*), with minor modifications to the source code (supporting USB video class, UVC, camcorders and the High Sierra MacOS) and user interface (allowing manual manipulations to recording duration). A dose-response titration (10 μM – 0.156 μM) of CB-5083 and NMS-873 was performed to assess adult worm anti-schistosomal potencies. Each titration point was performed in triplicate (a pair of worms for each replicate). Worm movement was recorded with WormassayGP2, as mentioned above. Mean motility scores were calculated for each titration point and dose-response curves were derived in comparison to worms co-cultured in DMSO (0.1% v/v; negative control; 100% motility) and PZQ (10 μM in 0.1% DMSO; positive control; 0% motility). Anti-schistosomula activities of the selected compounds were assessed using the high-content imaging platform Roboworm as previously described (*32, 34*). Compounds (reconstituted in dimethyl sulfoxide, DMSO; 10 mM stock concentration) were initially tested at two different concentration points (10 μM and 50 μM, in 0.625% DMSO) along with negative (0.625% DMSO) and positive controls (PZQ at 10 μM final concentration in 0.625 % DMSO). Schistosomula/compound co-cultures were then incubated at 37ºC for 72 h in a humidified atmosphere containing 5% CO_2 before phenotype and motility metrics were assessed. Two-fold titrations (10 μM, 5 μM, 2.5 μM, 1.25 μM and 0.625 μM) were subsequently conducted for all compounds consistently identified as hits at 10 μM in the primary screens. Single point schistosomula screens (10 μM) were repeated three times whereas dose response titrations were performed twice (in each screen two technical replicates were included). Phenotype and motility scores deriving from the titration of each compound were collected to generate approximate EC_{50}s using GraphPad Prism. To quantify adult worm attachment to the substrate following drug treatment, freshly perfused adult worms were sorted into a 6-well plate with 3 mL Basch 169 media and cultured overnight. The following day (D0) unattached worms removed and compounds were added to the media to a final concentration of 10 μM. Media and drug were replaced on D1 and D2. Media with no drug was added on D3 and D5. Parasite attachment was monitored from D0 to D7.

RNAseq for *stk25* and *tao* RNAi-treated worms

To examine gene expression changes following loss of *tao* or *stk25*, 10 adult worm pairs were placed into 6-well plates and cultured in 3 mL Basch 169 supplemented with 30 μg/mL dsRNA for 3 days. Media and dsRNA were replaced daily. On D3, dsRNA-containing media was removed and worms were maintained in 6 mL Basch 169 media that was replaced every other day. On day 6 (*tao(RNAi)*) or D9 (*stk25(RNAi)*) worms were anesthetized with 0.25% tricaine and separated by sex. As controls, worms cultured in parallel were treated with an irrelevant dsRNA (*2*). Three biological replicates were performed for each knockdown condition and their respective control treatment. For RNA extraction, male worms were collected, excess media removed, and 100 μL of TRIZOL was added. Parasites were then flash frozen in liquid N_2,

homogenized with a micro pestle, the volume of TRIZOL was brought to 600 μL before RNA was purified using a Zymo Direct-zol RNA miniprep kit and processed for Illumina sequencing. RNAseq data across the three biologically independent replicates for each knockdown set was mapped to the *S. mansoni* genome (v7) using STAR and differential expression was analyzed by DESeq2 as previously described (*35*). Raw data can be accessed in NCBI under the accession number GSE146720. To define the correlation between genes differentially regulated following RNAi of *tao* and/or *stk25*, we compiled a list of all genes that had significantly changed expression in either *stk(RNAi)* or *tao(RNAi)* datasets and plotted their log2 fold-change expression in GraphPad Prism to calculate a Pearson correlation coefficient. To evaluate the effects of *tao* and *stk25* RNAi on gene expression in specific tissues and cell types we collapsed related cell types from a *S. mansoni* single cell atlas (*17*) into 10 broad clusters of somatic cell types found in male worms (muscles, neurons, neoblasts, gut, etc.) (**Fig. S10B**). Genes highly enriched in these clusters were determined using Seurat v3.1.1(*36*) (parameters = logfc.threshold = 1, min.pct = 0.5) and compared to genes down-regulated ($p\ adj < 0.000001$) following both *tao* and *stk25* RNAi.

Purification of Recombinant STK25 and TAO

Baculovirus expressing wildtype *Schistosoma mansoni* Smp_068060 (TAO) or Smp_096640 (STK25) with a C-terminal His_6 tag was generated by GenScript (Piscaaway, NJ). cDNA encoding kinase-dead versions of both kinases were subcloned into the pFastBac1 vector with C-terminal His_6 tag and baculovirus was generated according to the manufacturer's instructions using the Bac-to-Bac Baculovirus Expression System (Invitrogen). Baculovirus was used as a 3rd pass virus to infect Sf9 cells grown in Gibco Sf 900 III SFM (Thermofisher Scientific) supplemented with 1% FBS and Antibiotic-Antimycotic solution (Sigma-Aldrich). Cells were harvested 72 hrs post infection for SmSTK25 expression and 48 hrs post infection for SmTAO expression. Frozen cell pellets were lysed with 20 mM Tris, pH 8.0, 5 mM $MgCl_2$, 300 mM NaCl, 1% Triton X-100 (Fisher Scientific), DNase (24 μg/mL), 10% glycerol, 3 mM 2-mercaptoethanol, and protease inhibitors (1 μg/mL aprotinin, 2 μg/mL leupeptin, 1 mM benzamidine, and 0.2 mM PMSF). After homogenization, the suspension was centrifuged for 1 h at 186,000 × *g* and the supernatant was rotated with Ni^{2+}-NTA resin (Qiagen) for 1.5 hrs. The resin was washed, and the protein was eluted in 20 mM Tris, pH 8.0, 5 mM $MgCl_2$, 300 mM NaCl, 0.05% Triton X-100, 10% glycerol, 3 mM 2-mercaptoethanol, 150 mM Imidazole, pH 8.0 and protease inhibitors (1 μg/mL aprotinin, 2 μg/mL leupeptin, 1 mM benzamidine, and 0.2 mM PMSF). Eluted proteins were either flash frozen or further dialyzed overnight into storage buffer (20 mM Tris, pH 8.5, 5 mM $MgCl_2$, 150 mM NaCl, 0.5 mM DTT, 10% glycerol, and 1 mM benzamidine) and flash frozen to -80°C.

To generate an anti-SmSTK25 antibody, a C-terminal fragment of SmSTK25 corresponding to AA513-622 was amplified and sub-cloned into pET28 vector with a C-terminal His_6 tag for expression in *Escherichia coli.* This fragment was purified from transformed Rossetta 2 cells grown in LB medium and induced with 1mM isopropyl 1-thio-β-D-galactopyranoside for 16 hrs at 18°C. Cells were pelleted and resuspended into lysis buffer containing 50 mM Tris, pH8.0, 300 mM NaCl, 10% glycerol, and protease inhibitors (0.2 mM PMSF, 2 μg/mL aprotinin, and 2 μg/mL leupeptin). The suspension was freeze-thawed and the following reagents were added to a final concentration of 1 mg/mL lysozyme, 1% Triton X-100, 5 μg/mL DNase. After homogenization and sonication, lysate was centrifuged for 40 min at 186,000× *g,* and rotated with Ni^{2+}-NTA resin for 1.5 hrs. The resin was washed, and protein was eluted in lysis buffer containing 300 mM imidazole. SmSTK25 (513-622) was buffer-exchanged into 1× PBS and 10% glycerol and applied to a Superdex 200 column for gel filtration chromatography on an AKTA FPLC. The sample was processed at a flow rate of 0.9 mL/min in 1× PBS and 10% glycerol. Eluate was collected as 90 1-mL fractions on a Frac 900 fraction collector (Amersham Pharmacia) maintained at 4°C. Each fraction was assessed for protein and concentrated with an Amicon concentrator, 10-kDa cut-off (Millipore). Rabbit polyclonal antibodies were generated by Cocalico Biologicals, Inc and confirmed to recognize the recombinant schistosome STK25 by western blot.

Evaluation of kinase activity

For kinase assays with radiolabeled ATP, STK25 or STK25K48R (1.7 μM) were incubated alone or together with either TAO or TAOK57R (0.3 μM) and 50 μM ATP ([γ-^{32}P]ATP, 6,000-9,000 cpm/pmol) in 10 mM Tris, pH 8.0, and 10 mM $MgCl_2$ for 10 min at 30°C. Following gel electrophoresis and autoradiography, STK25 or STK25K48R (1.25 μM) as well as TAO or TAOK57R (0.25 μM) bands were excised and analyzed by scintillation counting (Perkin Elmer, Tri-Carb 2910TR). For evaluation of STK25 phosphorylation by western blotting, proteins were incubated for 30 mins at 30°C in kinase assay buffer (10 mM Tris pH 8.0, 10 mM $MgCl_2$, 0.5 μM per protein) with or without 50 μM ATP in a reaction volume of 30 μL. Reactions were quenched with 10 μL of 4× Laemmli buffer and samples boiled at 99°C for 4 min, then stored at -20°C. Proteins were resolved by SDS-PAGE (Bio-Rad 4-20% precast polyacrylamide gel, cat# 4568095) for 45 min at 140 V. The gel was placed in cold transfer buffer (25 mM Tris, 192 mM Glycine, 10% (v/v) methanol, pH ~8.4) and transferred to a nitrocellulose membrane (Bio-Rad cat# 1620115) for 60 min at 100 V, 4°C. The membrane was stained with Ponceau S Solution (Sigma cat# P7170) for 5 min, imaged and destained by 2× washes with TBST (20 mM Tris, 150 mM NaCl, 0.1% (v/v) Tween20). The membrane was blocked for 1 hr at RT with blocking buffer (Odyssey Blocking Buffer, Li-Cor cat# 927-40000) diluted 1:5 in TBS (20 mM Tris, 150 mM NaCl)), then stained O/N at 4°C with primary antibody diluted in blocking buffer. Membrane was washed 3× 5 min with TBST, then stained with secondary antibody diluted in blocking buffer, 1 hr at RT. Membrane was washed 3× 5 min with TBST, then imaged with a LI-COR Odyssey imaging system. Primary antibodies were as follows: to detect phosphorylated T173 of smSTK25 and kinase-dead smSTK25, we used Rabbit-anti-MST4 + MST3 + STK25 (phospho T174 + T178 + T190) antibody [EP2123Y] (ab76579) from Abcam. To detect total smSTK25 and kinase-dead smSTK25 we used the Rabbit polyclonal antibody against the STK25 C-terminus described above. Secondary antibody for all blots was LI-COR IRDYE 680 red, Goat anti-Rabbit cat# 925-68071, and was used at a dilution of 1:10,000.

For mass spectrometry analyses of SmTAO phosphorylation of kinase-dead SmSTK25, kinase reactions were performed as above, and the SmSTK protein was excised from an SDS-PAGE gel and the protein was analyzed by the UT Southwestern Proteomics Core. Specifically, protein gel pieces were digested overnight with trypsin (Pierce) following reduction and alkylation with DTT and iodoacetamide (Sigma–Aldrich). The samples then underwent solid-phase extraction cleanup with Oasis HLB plates (Waters) and the resulting samples were analyzed by LC/MS/MS, using an Orbitrap Fusion Lumos mass spectrometer (Thermo Electron) coupled to an Ultimate 3000 RSLC-Nano liquid chromatography systems (Dionex). Samples were injected onto a 75 μm i.d., 75-cm long EasySpray column (Thermo), and eluted with a gradient from 1-28% buffer B over 90 min. Buffer A contained 2% (v/v) ACN and 0.1% formic acid in water, and buffer B contained 80% (v/v) ACN, 10% (v/v) trifluoroethanol, and 0.1% formic acid in water. The mass spectrometer operated in positive ion mode with a source voltage of 1.8 kV and an ion transfer tube temperature of 275 °C. MS scans were acquired at 120,000 resolution in the Orbitrap and up to 10 MS/MS spectra were obtained in the ion trap for each full spectrum acquired using higher-energy collisional dissociation (HCD) for ions with charges 2-7. Dynamic exclusion was set for 25 s after an ion was selected for fragmentation. Raw MS data files were converted to a peak list format and analyzed using the central proteomics facilities pipeline (CPFP), version 2.0.3 (*37, 38*). Peptide identification was performed using the X!Tandem (*39*) and open MS search algorithm (OMSSA) (*40*) search engines against the *S. mansoni* protein database from Uniprot, with common contaminants and reversed decoy sequences appended (*41*). Fragment and precursor tolerances of 10 ppm and 0.6 Da were specified, and three missed cleavages were allowed. Carbamidomethylation of Cys was set as a fixed modification with oxidation of Met and phosphorylation of Ser, Thr, and Tyr set as variable modifications. Phosphorylation sites were localized using the ModLS algorithm, using cutoff values for positive site identification that represent a scenario where the false discovery rate is < 1% (*42*).

Gene Ontology (GO)

The Gene Ontology (GO) annotation for *Schistosoma mansoni* was obtained from GeneDB (https://www.genedb.org/). GO term enrichment was performed using the weight01 method provided in topGO (v2.34.0) for biological process (BP), molecular function (MF) and cellular component (CC). GO term enrichment was performed by comparing hits with the entire list of 2,216 screened genes. For each category, the analysis was restricted to terms with a node size of >= 5. Fisher's exact test was applied to assess the significance of overrepresented terms compared with the screened genes. The threshold was set as FDR < 0.05.

Identification of *S. mansoni*-specific phenotypes

For data in Table S5, close homologs of *S. mansoni* genes in *C. elegans, D. melanogaster* and human were identified as *C. elegans* or *D. melanogaster* genes belonging to the same gene family, or listed as orthologs, in WormBase ParaSite v14 (*43*). We considered *S. mansoni* and *Schmidtea mediterranea* genes (taking the dd_Smed_v6 gene set from PlanMine (*44*)) to be one-to-one orthologs if they were each other's top BLASTP hits, with *E*-value < 0.05, and the BLAST *E*-value of the top BLASTP hit was 10^5 times lower than the BLAST *E*-value for the next best hit. *C. elegans* RNAi/mutant phenotypes were identified from WormBase (*45*) and *D. melanogaster* phenotypes from FlyBase (*46*), as of May 2020.

Fig. S1

A

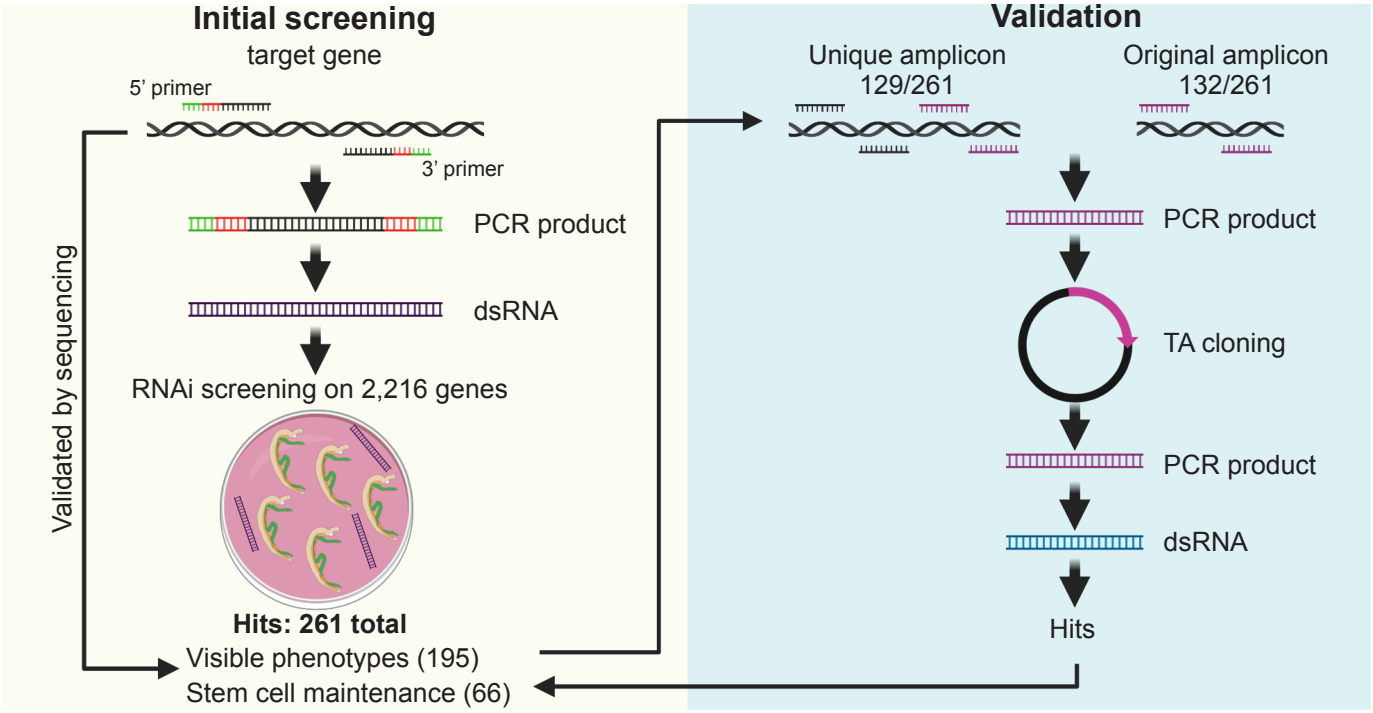

B

>Smp_002160

CTTCACGGTACCTAGGGGTTATTTTCACCTTTCTTTGCATTGTTTTTCAAACAATGGGTACTGCAATGGATGTCCTAGATATTCTCGATCTGAAGAAT-
CAAGTCCCAGAAAGTCTATGCTTGATAAAGAAGCTATTCTGAGTCGTGCAGAGAAAAGAAAGAGTTATCGTCCTAACCCACCACCAAAAAGGC-
CCGGTCATGTTCCTCGTGAAGTTTGGGGCTTACATAGCACTCTTAACAATAATCTTCCTCCGATTATGCCAACTGATAATACACCTCTTTATAAA-
C**AACCCAAAGCTGTGATTGGT**GTAGGACGAGTTCGTTCTTGGCAATGGACACCTTTTACAAATTCCGCTAGACAAGATAATCTAGTCTTATAT-
CATTGGAGACGAGAAAGCACTGATCCAGAGGCTAATAAAGATTATTATTTTGCACGATACAATAAGCATGTCACTGTTCCTGAATACACTGTAGAA-
GAGTACGAAACAATGCTAAAAGATCCAAAATGGAGTGAAGAGCGTACAGCACATTTGATGGAATTGGCTAAACGTTTTGATTTACGTTTTATTCATAT-
GAGAGATCGATGGGATTGTGAAAAGTTCCCTGGACGTCCATCGGTTGAAGATCTTAAAGAAAGATATTATGGAATTTTAACACAGTTAGATA-
AGGCTCGTGGAACAAATCTTTCACAAGGTCTAAGATATGATGCAGCACATGAACGTCGACGTAAACAACAATTAAGTTTACTTTATGGTCGTA-
CAAAAGATCAAGTTGAAGAAGAACAACGTTTAATTATGGAATTACGTAAAATCGAAGCTAGACGTAAAGAACGTGAACGTAAAAAACAAGATTTA-
CAAAAACTTATCTCATTGGCTGACAGTGTAACTCGGGATTGTGAATTATCTGAGCATACAGGTTATGAAACAAATACAGATGATACAAATTCTTG-
GCTTACA**TCTACACATTCGTCCGTTGG**CTGTGGTCTATCATCTTCCAATAATTCATTGTTAACATCAACAACACTAGCAGGAAATACTGGGTTA-
CAACGTAAGCGACCCGGTGGTGTTAGTGGTTTGAATGCTAGTAATAATAGTACTGGCAATATTACGTCATCGTCTAGTCAGTTAATTGGAAATA-
CAAATTCACTCATCAATACAGATTCTAGTTGTACGAGTTTAACCAGTACAGGAGCAGCTGGTAGCGCCAATACTGGAGCGGTGATATCCTCTG-
GAGATATTTGTGCTTCATTAAATTCTGCTTCGAATACAGCTAATACCGCATTGAATACACAATATTCAATAAACTTTTTGGATGTTAGCA**AAAATC-**
CCGGTGCTCATCTACGTAGTCAAAAGATGAAATTACCCAGTAATTTAGGACAGAAAAAGACAAGAATCATTGAAAACTTCTTAGGTCATTTA-
CAAATTGATCCTAATCCACCGGCAACTGCAGAAATTGTTGAAGCATATAATGGTTTACGTTCAAAAATTCTACTTTTATTCGATTTACGTCTAGC-
GTTATTAAATTGTGACTTTGAATTACATTCAGCTCGACTAAGACTAGAAACATTTGCTCCTAATAAACCGTTACCTTGTGGACTTGCTAGTCTGC-
CAAATCCTAGTGTATCAGAATCACCTGAAGATTCTTATTATAATTTAATCGATCCGTTGATTTTGTCGGCACTTCGTGTAGCCGACTCAAAACGTC-
CAATTCTACCGCGTCATTCACTTGGAGTTGCTGGTACATTGGCTGCGGCTGCTGGAAGTTTAGGTTTGCATAATATGACTAGTGGAAGTAGT-
GGTATTCCATCTACTAATACAACAGTGGAGAAATCAGATCCAAAACAATGTCGATTGAACCCATCGTCCATTGTTAATTCTTCAGATAGTGGA-
CAGTATAATTCTAGTGGATTGACAACTACTCGATCGTCTCCAGCGTTGTCAGGAGGCGGAGGCACTGGGAATCTAGATTCAGATAATTCGTCAT-
CAGCCGGAGATGG**TATCGGCAGTTCACAACGTC**GTAGAAGAGCAGCAGCTTTAGAACAGGGACGTGTTTTAAAGAAACTTAAAATTAAAGGA-
CAACTTGTTGATTGAAACTGTTGGTTGTGGAAAAACAAACAAATTTTTTGTTGTCTATGTGTACATAAAAATATTTTTTTGATTGATCTCATTTGATC-
TACCGTTTCAGAAGGAAACAGTTTCATAATAAATAGTTTTCCCTC

Initial primers

	T7 polymerase binding sequence	*NotI*	Gene-specific primer
Forward:	GAATTTAATACGACTCACTATAGGGCGGCCGC		AAAATCCCGGTGCTCATCTA
Reverse:	GAATTTAATACGACTCACTATAGGGCGCGCC		GACGTTGTGAACTGCCGATA
	T7 polymerase binding sequence	*AscI*	Gene-specific primer

Primers for validation

Forward: AACCCAAAGCTGTGATTGGT

Reverse:CCAACGGACGAATGTGTAGA

Fig. S1. Large-scale RNAi screening in *S. mansoni.* (A) Pipeline for large-scale RNAi screening . **(B)** An example of strategy for a single gene from the initial RNAi screen and the subsequent validation. PCR primers for the initial screening were modified by adding sequences including restriction enzyme sites (*NotI* on forward primer, *AscI* on reverse primer) and a T7 polymerase promoter on both forward and reverse primers. To validate PCR product sequences we digested with *NotI* and the amplicon was sequenced with a T7 primer. To validate the initial screening results, in 129 cases we cloned a cDNA fragment that did not overlap with the initial amplicon. In 132 cases we assessed potential off-target effects by BLAST searching against the *S. mansoni* transcriptome.

Fig. S2

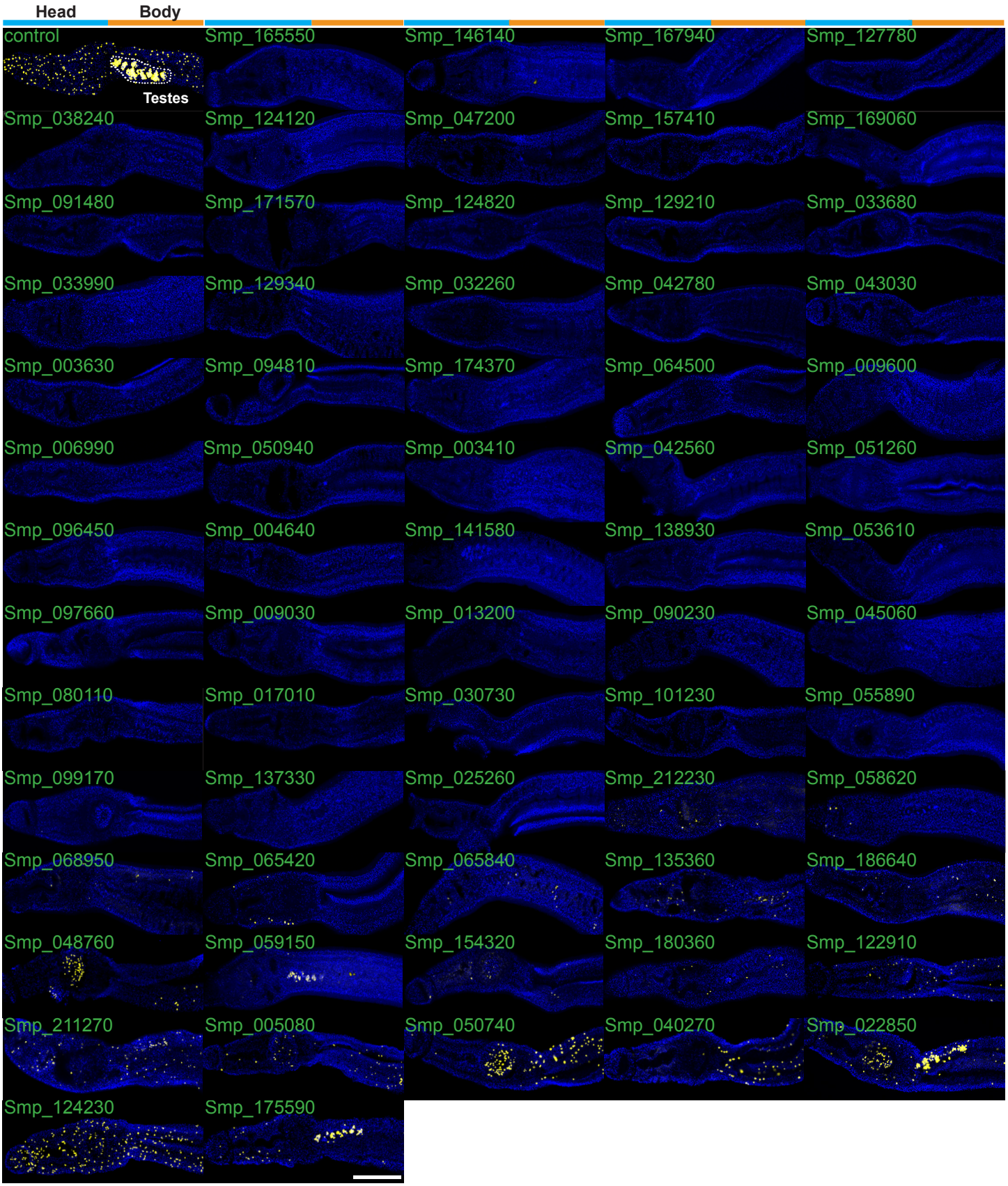

Fig.S2. All 66 hits with phenotypes of loss of stem cell maintenance. EdU labeling of proliferative cells in somatic tissues and the testes is shown in yellow, parasites are counterstained with DAPI to mark nuclei. RNAi of *DNA polymerase epsilon subunit* (Smp_124120) leads to loss of all proliferative cells, whereas *rad51* (Smp_124230) or *fgfrA* (Smp_175590) lead to a selective reduction in the testes and soma, respectively. Details of EdU staining for each hit are provided in Table S3. Scale Bar, 200 µm.

Fig. S3

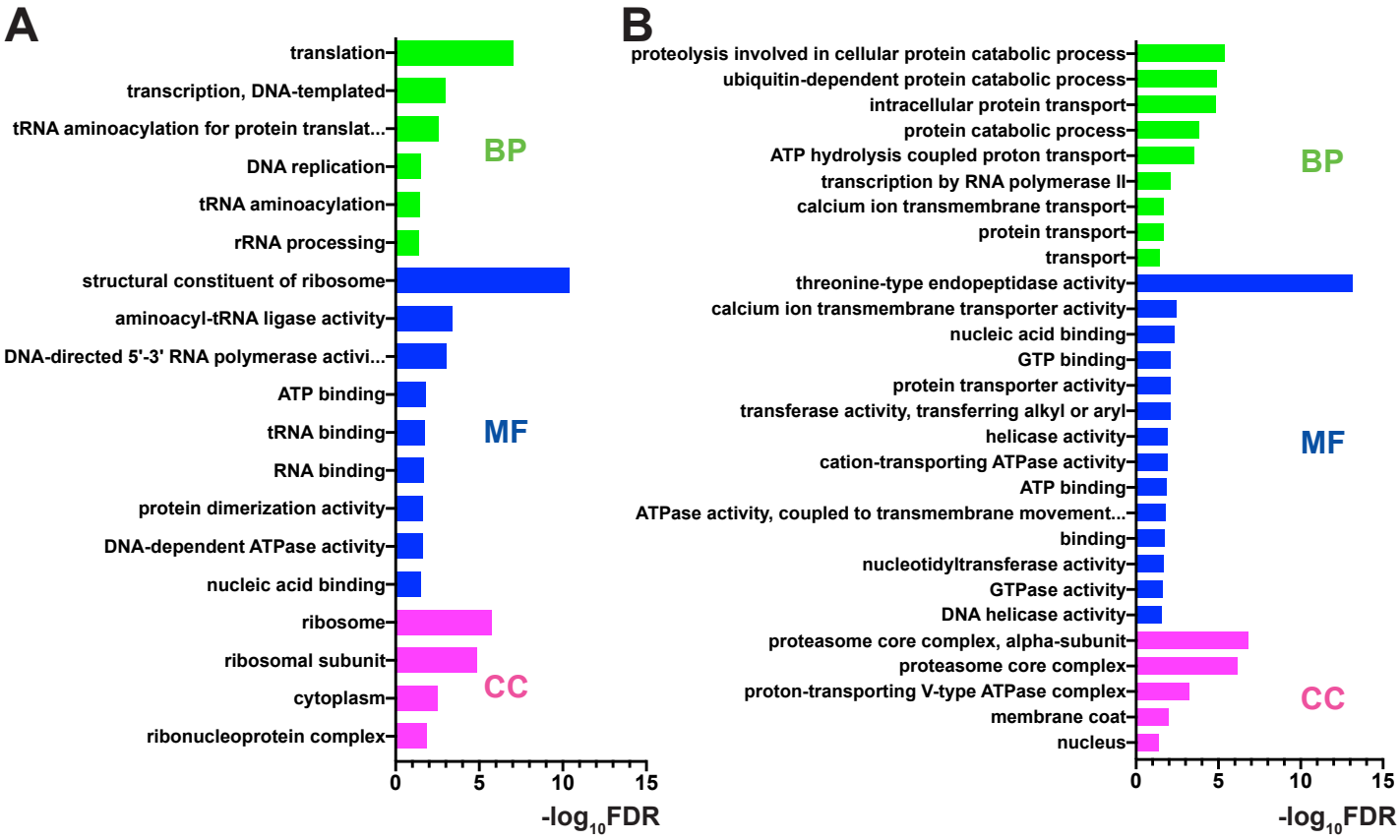

Fig. S3. Gene Ontology (GO) analysis. (**A**) GO analysis of all the 66 genes with a loss of stem cells phenotype. (**B**) GO analysis of all the 195 genes with a detachment phenotype. GO term enrichment was performed by comparing hits with the entire list of 2,216 screened genes. All enriched GO terms with the threshold FDR< 0.05 are listed for Biological Process (BP), Molecular Function (MF) and Cellular Component (CC).

Fig. S4

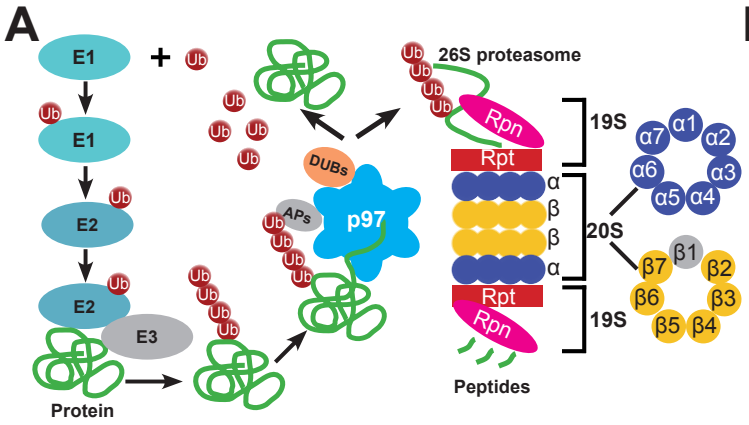

B

Ubiquitin system

Protein ubiquitination	Protein deubiquitination	Others
Smp_162630: E1	Smp_069960: DUBs	Smp_018240: p97
Smp_103710: E2	Smp_089180: DUBs	

26S proteasome

20S subunit		19S subunit
Smp_212920: α1	Smp_074500: β2	Smp_012470: Rpt1
Smp_067890: α2	Smp_121430: β3	Smp_175250: Rpn2
Smp_092280: α3	Smp_056500: β4	Smp_042270: Rpn3
Smp_070930: α4	Smp_212880: β5	Smp_178810: Rpn9
Smp_032580: α5	Smp_034490: β6	Smp_173840: Rpn10
Smp_207080: α6	Smp_073410: β7	
Smp_076230: α7		

C

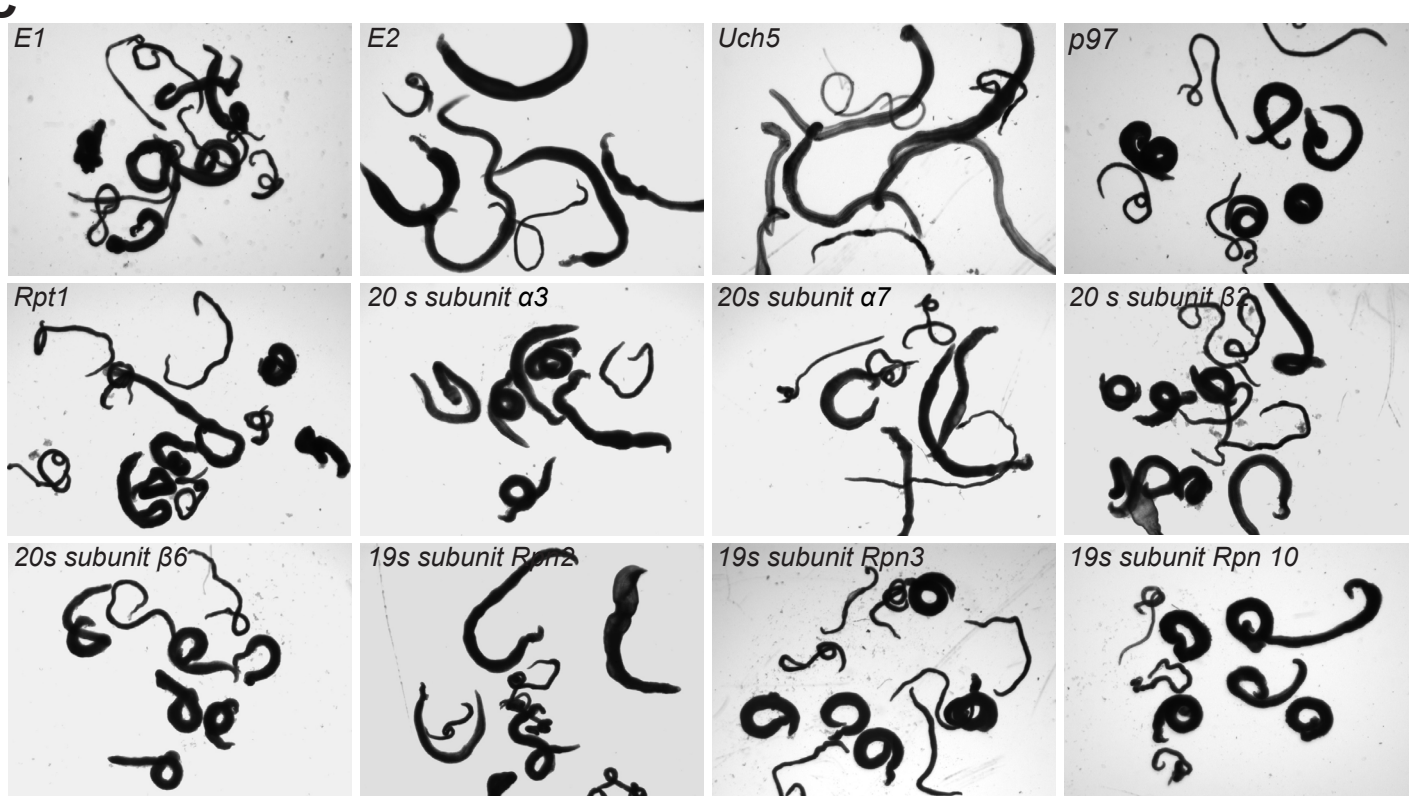

Fig. S4. Phenotypes of RNAi-treatment for various ubiquitin-proteasome system (UPS) components. (**A**) A large fraction of genes resulting in visible phenotypes were associated with components of the Ubiquitin Proteasome System (UPS). In the cartoon of the UPS, colored components correspond to genes associated with visible phenotypes. (**B**) List of genes associated with visible phenotypes and the component of the UPS they encode**.** (**C**) RNAi of the listed UPS components in our 30-day treatment regime resulted in degeneration of the parasite's tegument or detachment from the substrate. *Uch5* (Smp_069960) , a ubiquitin carboxyl-terminal hydrolase 5 homolog, represents a deubiquitinaiting enzyme (DUBs).

Fig. S5

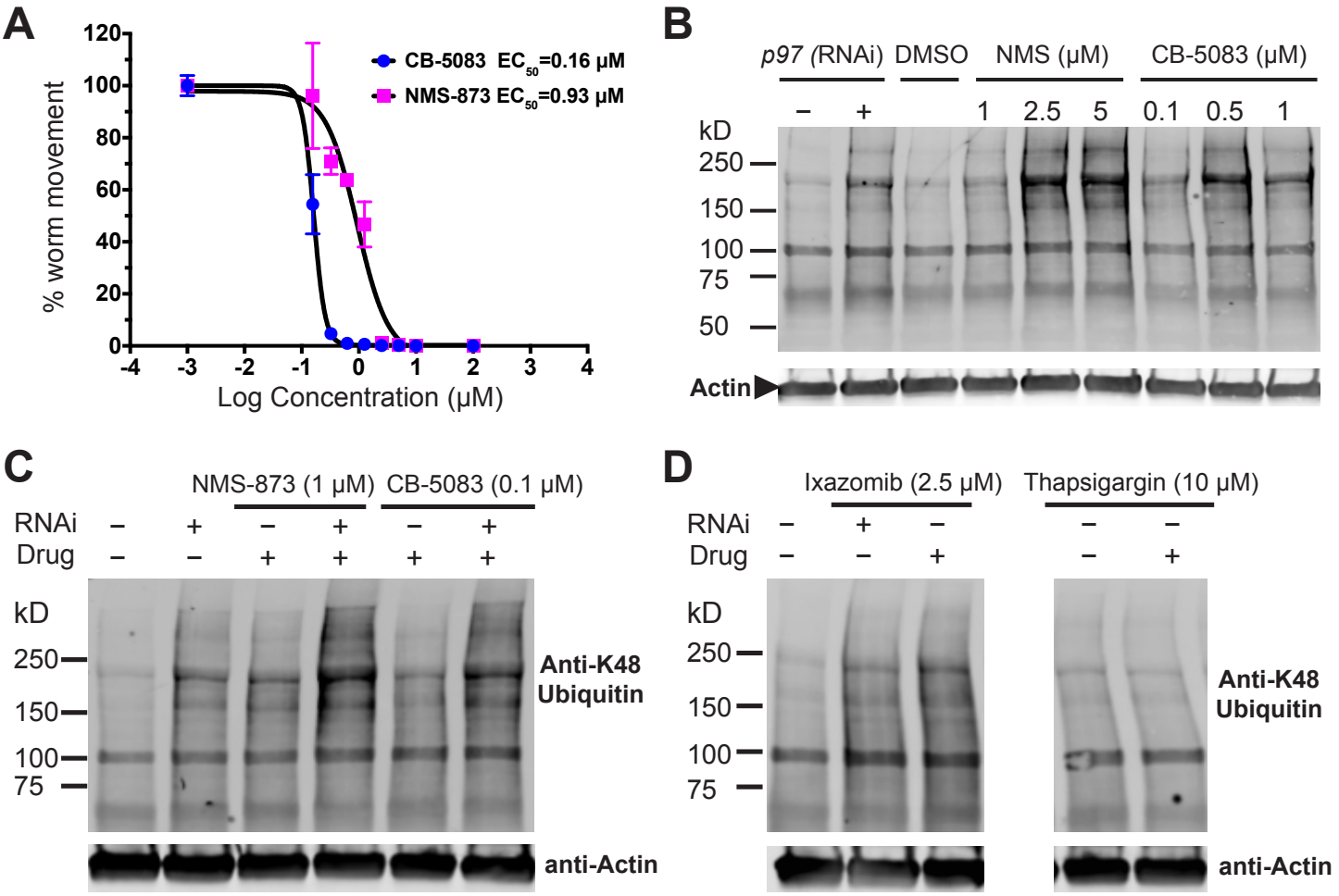

Fig. S5. Evaluation of p97/proteasome inhibitors. (**A**) EC50 values for the p97 inhibitors CB-5083 and NMS-873 on parasite movement. Error bars represent standard deviation of the mean motility scores (as percentages). n= 6 (three biological replicates, single adult worm pair/well for each concentration point). (**B**) Western Blot for K48-linked polyubiquitinated proteins. Representative from 3 experiments. (**C**) Western Blot for K48-linked polyubiquitinated proteins. RNAi of *S. mansoni p97* or treatment of worms with the p97 inhibitors caused an increase in the accumulation of K48-polyubiquitinated proteins. Representative from 3 experiments. (**D**) Western Blot for K48-linked polyubiquitinated proteins. RNAi of *S. mansoni proteasome subunit beta type-2* or treatment of worms with the proteasome inhibitor Ixazomib caused an increase in the accumulation of K48-polyubiquitinated proteins. Treatment of worms with non-UPS inhibitor thapsigargin, which also compromised worm vitality, did not increase the polyubiquitinated proteins. Representative image from 3 replicates.

Fig. S6

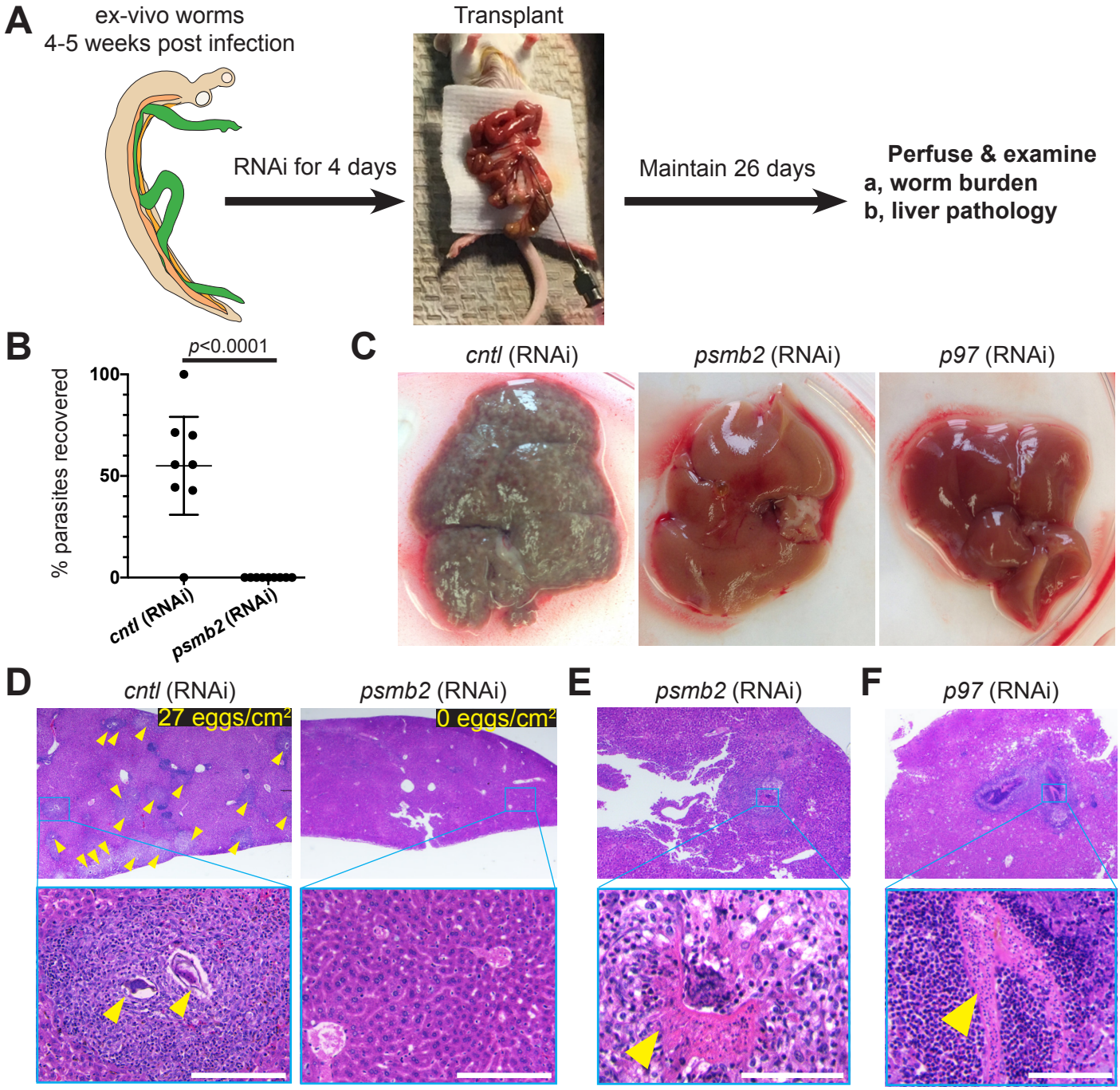

Fig. S6. *In vivo* validation of RNAi hits by surgical transplantation. (**A**) Strategy for *in vivo* validation. Parasites were perfused from mice at 4-5 weeks after infection and then treated with 30 μg/mL dsRNA for 4 days before surgical transfer into the mesenteric veins of naive mice. After 26 days, mice were sacrificed to harvest worms and livers. (**B**) Percent recovery of male parasites treated with dsRNA specific to *proteasome subunit beta type-2* (*psmb2*, Smp_074500; n = 10 transplants) or an irrelevant dsRNA (control; n = 8 transplants) following surgical transplantation of parasites into mice. ****, $p < 0.0001$, t-test. (**C**) Liver morphology of mice after transplantation of worms that were pretreated with control dsRNA, *proteasome subunit beta type-2 (psmb2) or p97* . Granulomas were only observed in mice receiving control parasites. (**D**) Hematoxylin and Eosin staining of livers from recipient mice that received either *control* or *psmb2* (RNAi). Schistosome egg-induced granulomas (indicated by yellow arrows) in livers were observed in *control* RNAi recipient mice, but not in *psmb2* (RNAi) recipient mice. Counts of eggs per liver section are shown in top right, n=3. (**E-F**) Transplanted parasites (indicated by yellow arrows) from RNAi treament of either proteasome *psmb2* (**E**) or *p97* (**F**) were found trapped and in various stages of degeneration in livers of recipient mice. Scale bars, 100 μm.

Fig. S7

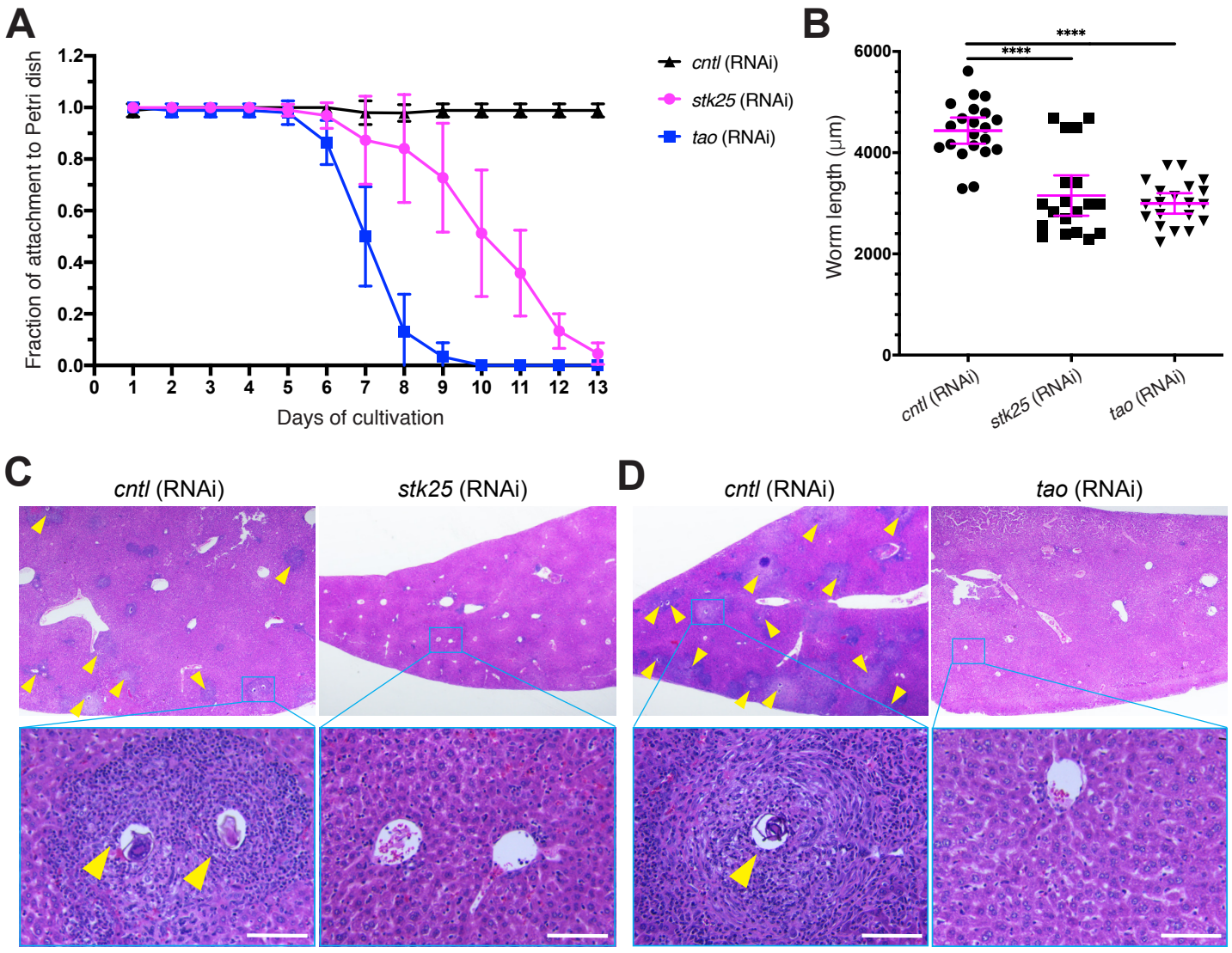

Fig. S7. Attachment curve of *stk25/tao* RNAi parasites *in vitro* and surgical transplantation of *stk25/tao* RNAi parasites. (**A**) dsRNA treatment of *S. mansoni* targeting either *stk25* or *tao* caused the worms to detach from Petri dish starting at 6 days after *in vitro* cultivation. *cntl*, control. n=9 for each group with 3 replicates. Error bars represent 95% confidence intervals. (**B**) *stk25* and *tao* RNAi-treated parasites are shorter than control RNAi-treated worms. >19 parasites monitored over 4 experiments. $p < 0.0001$, t-test. (**C**-**D**), Hematoxylin and Eosin staining of livers from recipient mice that received either *cntl* or *stk25* (RNAi) or *tao* (RNAi). Egg-induced granulomas (indicated by yellow arrows) were only observed in control group. n=3. Scale bars, 100 μm.

Fig. S8

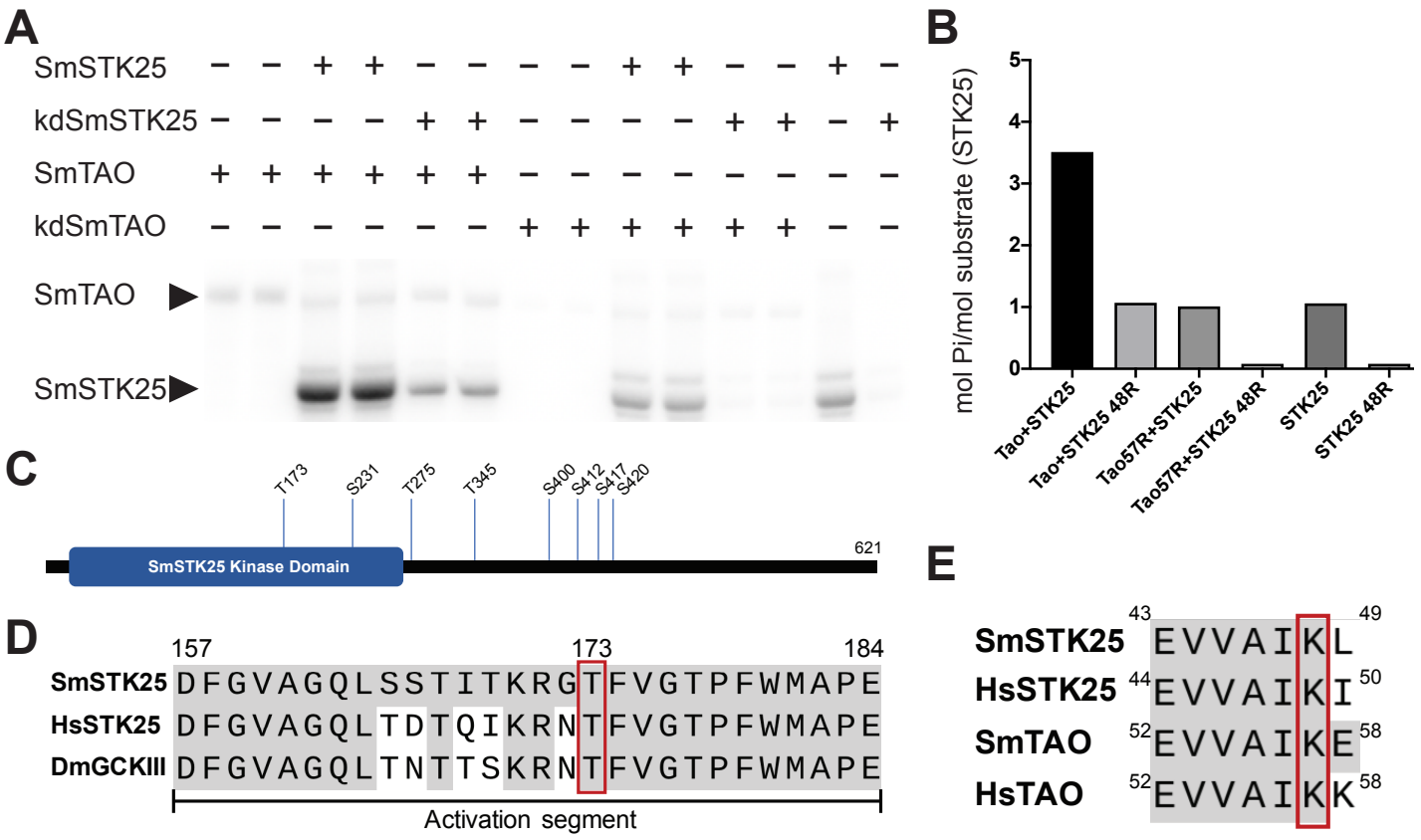

Fig. S8. Assays of *Schistosoma mansoni* protein kinases STK25 and TAO. (**A**) Autoradiography of a kinase assay with recombinant schistosome proteins. Wild type SmTAO protein phosphorylates both wild type and kinase-dead SmSTK25, and that signal is ablated when wild type SmTAO is replaced by a kinase-dead mutant (kdSmTAO, K57R). (**B**) Quantification of radioactive phosphate transfer in kinase assay shown in (**A**), by scintillation counting. Results from n = 2 technical replicates (**C**) High confidence phosphosites of SmSTK25 kinase from mass spectrometry. To determine high confidence sites, only those with ModLS scores >30 and ID prob >0.95 on the PTM (post-translational modification) report were chosen. Eight high confidence phosphosites were de-tected and shown on the cartoon. (**D**) Sequence alignment of *S.mansoni* STK25 kinase SmSTK25 activation segment and its human homologue HsSTK25 as well as *Drosophila* homologue DmG-CKIII. Threonine 173 (T173) indicated in red box is the phosphosite in the activation segment highly conserved in different organisms. The positions of amino acids on SmSTK25 were used. (**E**) Align-ment of amino acids surrounding the VAIK motif required for catalysis in most kinases. To make kinase dead versions of SmSTK25 and SmTAO, the catalytic lysine in the VAIK motif was mutated to arginine (K48R and K57R for SmSTK25 and SmTAO, respectively). Sm, *Schistosoma mansoni*; Hs, *Homo sapiens.*

Fig. S9

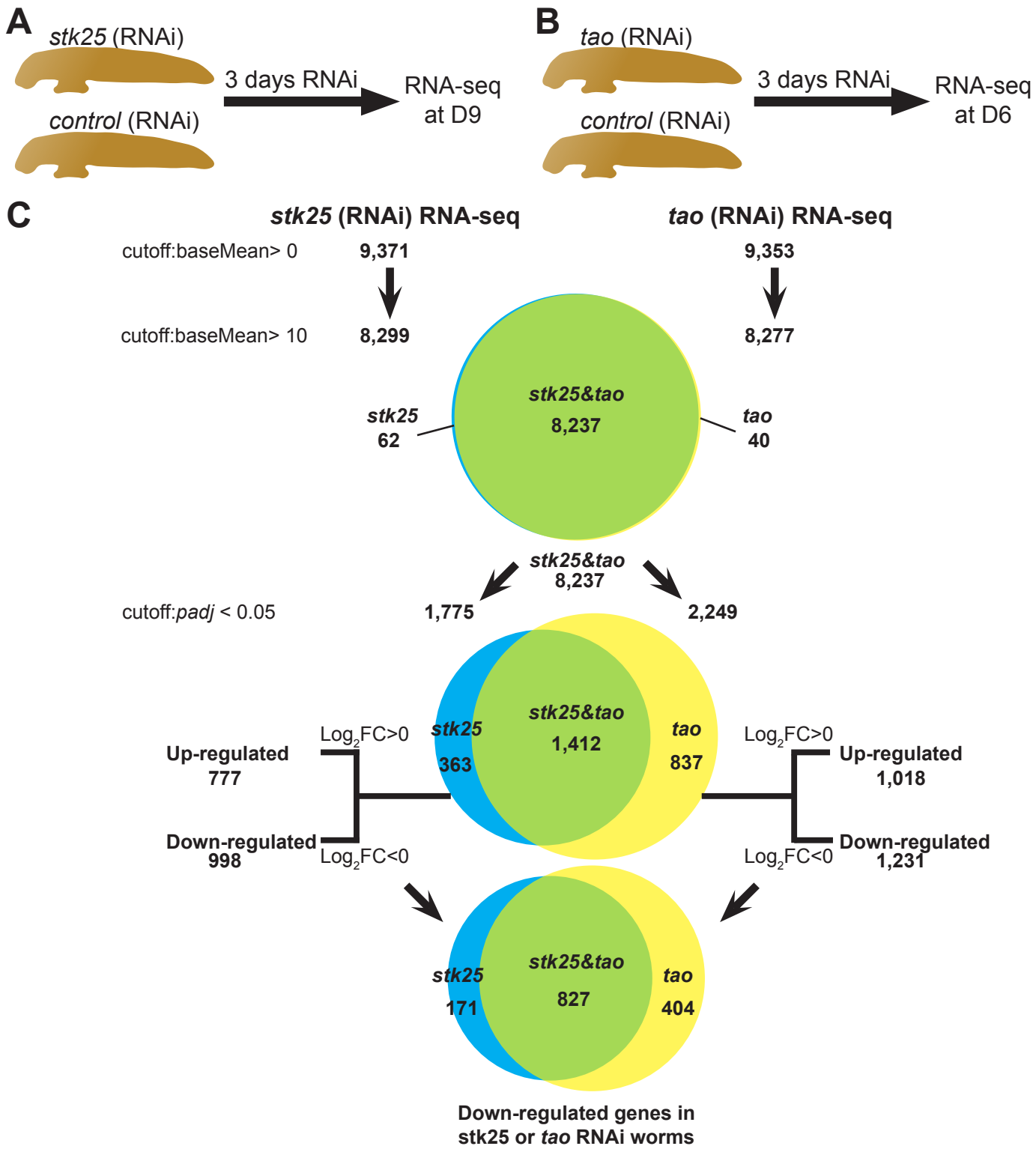

Fig. S9.RNA-seq and data analysis of the differentially expressed genes in *stk25/tao* RNAi. (**A**-**B**) RNAseq strategy for male worms treated with dsRNA that target either *tao* or *stk25*. (**C**) Analysis of the differentially expressed genes after *stk25* or *tao* RNAi. Genes with low expression level (baseMean≤ 10) were excluded before further analysis. Among the 8,237 genes that are both expressed in *stk25* and *tao* datasets indicated by Venn diagram, 1,775 genes and 2,249 genes were significantly differentially expressed (*padj* <0.05) in either *stk25* RNAi or *tao* RNAi compared with control RNAi worms. Of the 998 and 1,231 down-regulated genes (Log_2FC <0, *padj* <0.05) in *stk25* RNAi worms or *tao* RNAi worms, 827 were shared in both groups.

Fig. S10

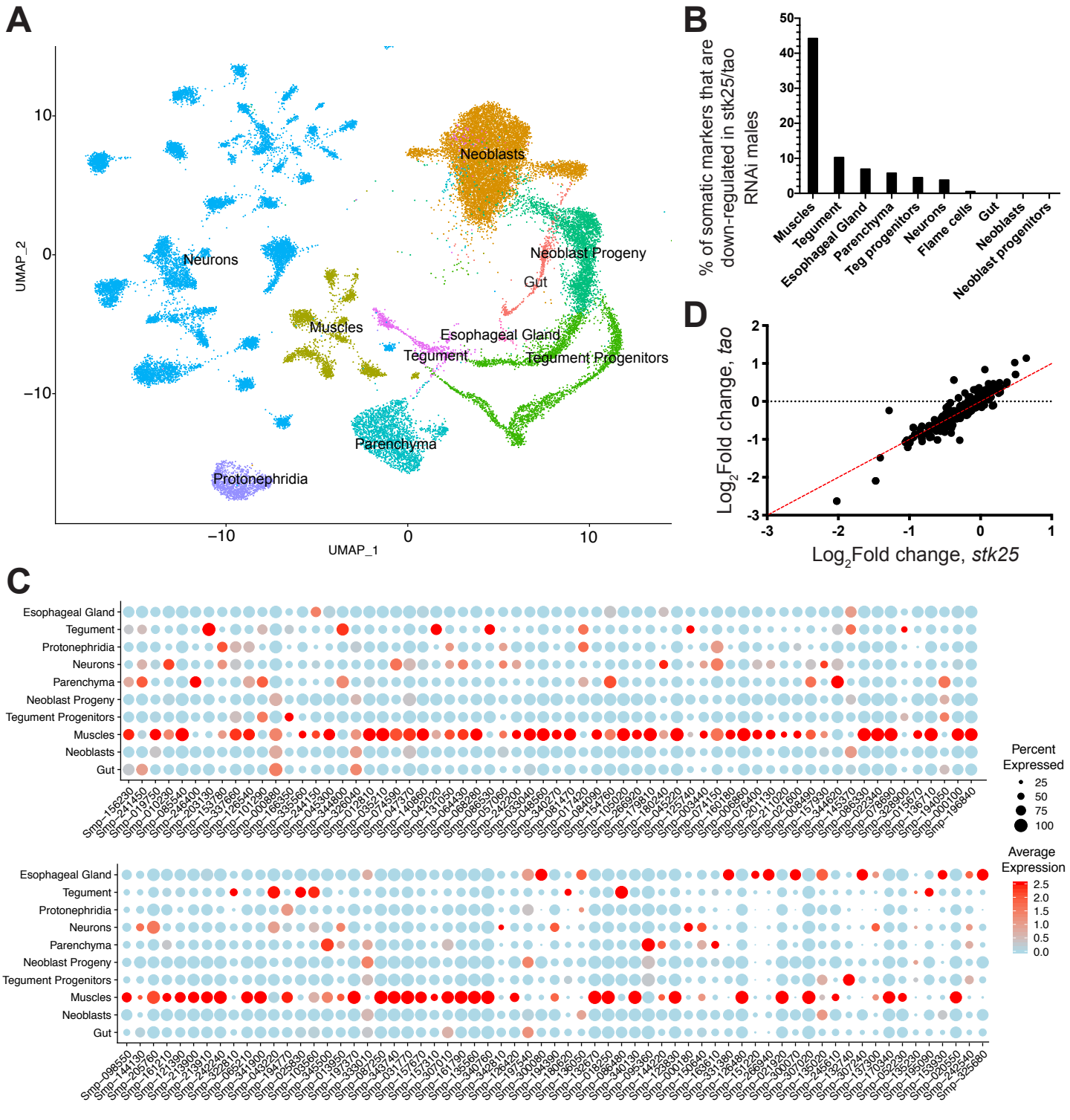

Fig. S10. Ratio of somatic markers in down-regulated genes in *stk25/tao* RNAi worms. (**A**) Dimensional reduction plot of somatic tissue clusters from an adult single cell atlas. Each dot represents a cell and cells from the same cluster were labeled with same color. (**B**) Percentage of tissue-specific somatic markers down-regulated (*padj* < 0.000001) after *stk25 or tao* RNAi treatment, measured by RNAseq. Nearly half of all muscle-specific markers are down-regulated in both *stk25 or tao* RNAi treatment groups. teg stands for tegument. (**C**) Dotplot showing the expression of the top 129 down-regulated (Log_2 Fold Change <-0.5, adjusted *p*-value < 0.00001) genes in common to both *stk25* and *tao* RNAi datasets across somatic tissues. Most down-regulated genes are expressed in muscles. (**D**) Scatter plot showing the relationship between all muscle-specific genes with baseMean>10 following either *stk25* or *tao* RNAi-treatment . These expression profiles were highly correlated (R=0.9, *p*<0.0001, Pearson correlation).

Fig. S11

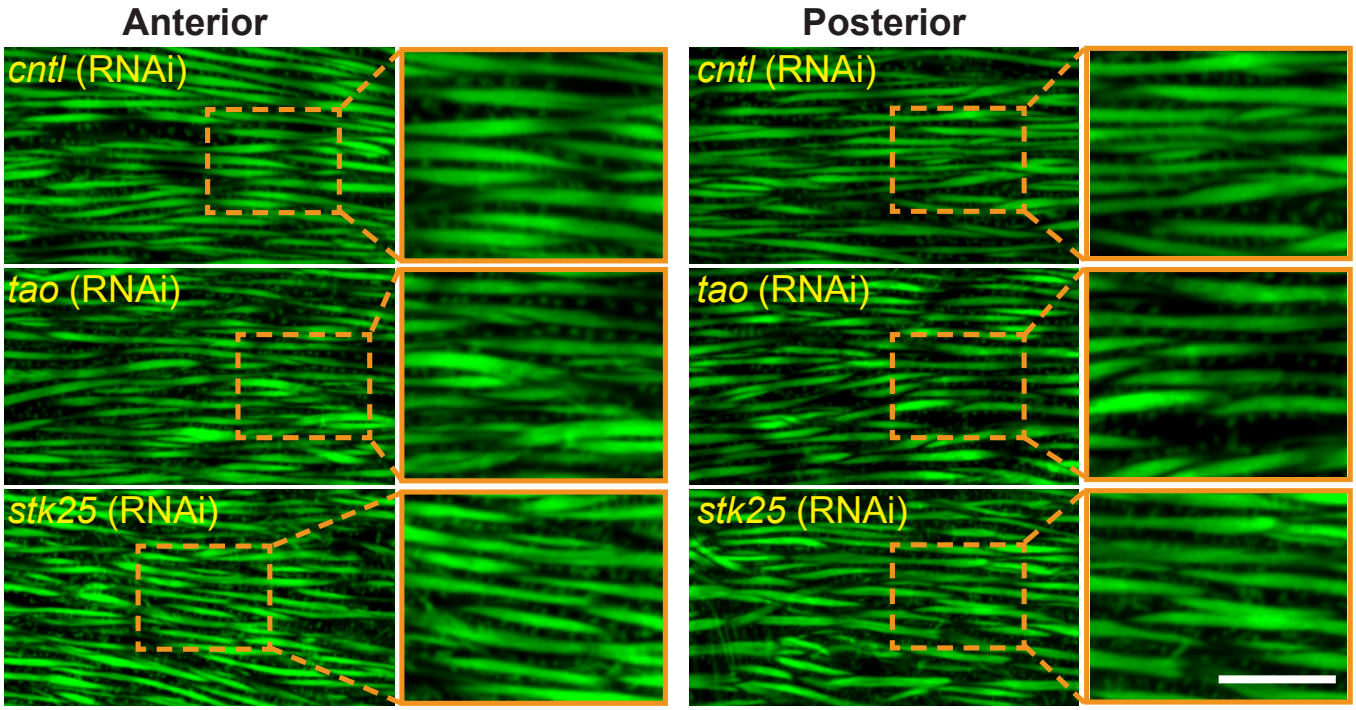

Fig. S11. Phalloidin staining of male parasites after RNAi treatment with either control (*cntl*), *tao* or *stk25* dsRNA. No obvious differences in muscle fiber morphology or numbers by phalloidin labeling were observed between *cntl* RNAi or *tao/stk*25 RNAi worms in either anterior (head) or posterior (body) parts of the worm body. Representative from n = 4 biological replicates Scale bar, 10 μm.

Captions for Tables S1-S10 (Tables are located in separate excel files)

Table S1. Information of 2,320 genes selected for RNAi screening.
Table S2. Details of 195 genes with detachment phenotypes.
Table S3. Details of 66 genes with phenotypes in EdU incorporation.
Table S4. Similarity of schistosome genes with phenotypes with gene products from other organisms by BLAST (*E*-value < 0.05) or orthologs present in Wormbase Parasite (*S. japonium* and *S. haematobium*).
Table S5. *S. mansoni* genes with detachment phenotypes compared to phenotypes of genes from *C. elegans* and *D. melanogaster* in WormBase/FlyBase
Table S6. *S. mansoni* RNAi hits and their potential inhibitors.
Table S7. Details of 14 selected inhibitors to test on schistosomes.
Table S8. Evaluation of compound activity on schistosomula
Table S9. Analysis of transcriptional changes following *stk25* or *tao* RNAi treatment by DESeq. Second tab shows in which somatic cell clusters the most down-regulated (p<0.00001 Log_2 Fold Change <-0.5) genes following *stk25* or *tao* RNAi treatment are expressed.
Table S10. Analysis of expression of somatic tissue-specific markers following *stk25* or *tao* RNAi treatment. Tissue-specific markers down-regulated (Log_2 Fold Change < 0 and *p adj* < 0.000001) following both *stk25* and *tao* RNAi-treatments are highlighted in red.

Captions for Movies S1-S4 (Movies are located in separate .mov file)

Movie S1. Adult worms after 30 days of i*n vitro* treatment with control dsRNA. On day 30, worms were physically active and firmly attached to the bottom of the dish.

Movie S2. Effects of various compounds on parasites. Parasites were treated with compounds for 72 hours at a concentration of 10 μM. We observed various worm defects ranging from death, to tissue degeneration, and detachment from the substrate. DMSO and PZQ were used as negative and positive controls, respectively.

Movie S3. Parasites died in 72 hours *in vitro* following treatment with CB-5083 or NMS-873. Adult worms were dead following 72 hours of treatment with 1 μM CB-5083 or 5 μM NMS-873. Tegumental damage was observed on these worms. DMSO was used as a control.

Movie S4. *stk25/tao* RNAi treated worms become hypercontracted and paralyzed by D13 following dsRNA treatment.